INTERACTION OF MAGNETIC NANOPARTICLES WITH POLYMERSOMES FOR USE AS MULTIMODAL NANOCARRIERS

by

Gizem Uysal

B.S., in Chemistry, Yıldız Technical University, 2020

Submitted to the Institute of Biomedical Engineering
in partial fulfillment of the requirements
for the degree of
Master of Science
in
Biomedical Engineering

Boğaziçi University
2023

INTERACTION OF MAGNETIC NANOPARTICLES WITH POLYMERSOMES FOR USE AS MULTIMODAL NANOCARRIERS

APPROVED BY:

Assist. Prof. Dr. Banu İyisan (Thesis Advisor)	.....
Prof. Dr. Bora Garipcan	.....
Assoc. Prof. Dr. Emine Ülkü Sarıtaş Çukur	.....

DATE OF APPROVAL: 15.08.2023

ACKNOWLEDGMENTS

"Science is the most real guide for civilization, for life, for success in the world" – Mustafa Kemal Atatürk.

First and foremost, I am deeply honored to be guided by the principles of Mustafa Kemal Atatürk, who emphasized the importance of science and reason in building the foundation of our nation.

I would like to express my deepest respect and appreciation to Assist.Prof.Dr.Banu İyisan, whose exceptional assistance was crucial to the success of this project. The scientific excellence, leadership and knowledge of Dr.İyisan were a light that motivated me for the success of this journey. Dr.İyisan is not only an advisor but also a role model and source of inspiration. Additionally, I extend my sincere gratitude to BINDLAB members for their unwavering support throughout this thesis.

I would like to express my deep appreciation to Prof.Dr.Dietmar Appelhans and Prof.Dr.Brigitte Voit providing an unparalleled scientific experience and opportunities. During my time at the Leibniz-Institut für Polymerforschung Dresden, Dr.Appelhans' constant support and confidence have tremendously benefited my academic endeavor.

The presence and constant support of my family Özge Gençler and Sadiye Gençler gave me strength in all areas of my life. Additionally, Words are not enough to express my gratitude to my faithful friends Meks,Muko and Fero who are always by my side, their presence brought much-needed peace and joy to this challenging process.

Lastly, I reserve special words of gratitude for my partner, Güneş Hasgören. Each line of this study carries the traces of the support and inspiration she provided. Her incredible support and infinite patience in my pursuit of scientific goals have constantly propelled me forward.

This study was supported by the Scientific&Technological Research Council of Turkey (TÜBİTAK) (Project Number 121C205)

Some part of this research were conducted at the Leibniz-Institut für Polymerforschung Dresden e.V. Additionally, Leibniz-Institut für Polymerforschung Dresden e.V. provided the necessary polymers and also financed a part of this research.

ACADEMIC ETHICS AND INTEGRITY STATEMENT

I, Gizem Uysal, hereby certify that I am aware of the Academic Ethics and Integrity Policy issued by the Council of Higher Education (YÖK) and I fully acknowledge all the consequences due to its violation by plagiarism or any other way.

Name :

Signature:

Date:

ABSTRACT

INTERACTION OF MAGNETIC NANOPARTICLES WITH POLYMERSOMES FOR USE AS MULTIMODAL NANOCARRIERS

Magnetic nanoparticles (MNPs) are extensively used targets for drugs to help with early detection and the treatment of disease. However, drug targeting with MNPs in a specific site within the body is quite challenging to achieve. In these situations, pH-responsive polymersomes can provide an effective dual targeting opportunity by hosting both MNPs on their membrane and drugs in the core. Therefore, the overarching objective of this research is to develop pH-sensitive polymersome that interacts with Super Paramagnetic Iron Oxide Nanoparticles (SPIONs), intended for potential applications. SPIONs were chosen as magnetic nanoparticles since they have good biocompatibility. We hypothesize that, in an acidic environment, increased permeability of pH-sensitive polymersomes induces controlled release from the core; meanwhile guiding with MNPs makes these structures a multimodal tool. In our first aim, we will synthesize SPIONs with average sizes of 10-15 nm using the co-precipitation method. These SPIONs will be stabilized with β-Cyclodextrin. Following that, Poly (ethylene glycol) (PEG), 2-(diethylamino)ethyl methacrylate (DEAEMA) and Ferrocene units will form the multimodal polymeric nanocarrier system. After polymersome formation, SPIONs will be introduced to the system, aiming for interaction with the exterior of the polymersome membrane facilitated by the complexation of ferrocene and β-Cyclodextrin. Our second aim involves conducting a morphological analysis of these multimodal nanocarriers to ensure their integrity and assess the success of the interaction. The ultimate prospective of this study is to utilize these multimodal nanocarriers for image-guided applications, potentially extending their use to drug loading in future studies.

Keywords: β-Cyclodextrin, Magnetic Nanoparticles, Nanobiotechnology,Polymersome, Iron Oxide

ÖZET

MANYETİK NANOPARÇACIKLARIN POLİMERZOMLARLA ETKİLEŞİMİNİN MULTİMODAL NANOTAŞIYICI OLARAK KULLANIMI İÇİN İNCELENMESİ

Manyetik nanoparçacıklar (MNP'ler), hastalıkların erken teşhisine ve tedavisine yardımcı olmak için yaygın olarak kullanılan ajanlardır. Ancak, vücuttaki belirli bir bölgede MNP'ler ile ilaç hedeflemeyi başarmak oldukça zordur. Bu durumlarda, pH'a duyarlı polimerlerzomlar, hem MNP'leri membranında hem de ilaçları çekirdekte barındırarak etkili bir ikili hedefleme fırsatı sağlayabilir. Bu nedenle, bu araştırmanın genel hedefi, potansiyel uygulamalar için süperparamanyetik demir oksit nanoparçacıkları (SPION'lar) ile etkileşime giren pH'a duyarlı polimerik nanotaşıyıcı sistemler tasarlamaktır. SPION'lar, diğer kontrast maddelerden daha iyi bir biyouyumluluğa sahip oldukları için çalışmanın manyetik nanoparçacıkları olarak seçilmiştir. Hedefimiz, 10-15 nm boyutlara sahip SPION'ları birlikte çöktürme yöntemi ile sentezlemektir. Bu SPION'lar sonrasında β-Siklodekstrin ile stabil hale getirilecektir. Bunu takiben, poli(etilen glikol) (PEG), 2-(dietilamino)etil metakrilat (DEAEMA) ve ferrosenden oluşan polimerzom geliştirilecektir. Sonrasında, SPION'lar polimerzoma dahil edilerek ferrosen ve β-Siklodekstrin yapıları arasında kompleks oluşması sağlanacaktır. İkinci hedefimiz, bu multimodal nanotaşıyıcıların morfolojik analizini gerçekleştirmek ve etkileşimlerinin başarısını değerlendirmektir. Bu çalışmanın sonraki aşamasında, bu multimodal nanotaşıyıcıların görüntüleme uygulamaları için kullanılması ve gelecekteki çalışmalarda ilaç yüklemeye genişletilmesi öngörülmektedir.

Anahtar Sözcükler: β-Siklodekstrin, Manyetik Nanoparçacık, Nanobiyoteknoloji, Polimerzom, Demir oksit

TABLE OF CONTENTS

ACKNOWLEDGMENTS iii
ACADEMIC ETHICS AND INTEGRITY STATEMENT v
ABSTRACT vi
ÖZET vii
LIST OF FIGURES xi
LIST OF TABLES xiii
LIST OF SYMBOLS xiv
LIST OF ABBREVIATIONS xv
1. INTRODUCTION 1
1.1 Motivation and Aim 1
1.2 Objectives 2
1.3 Thesis Outline 3
2. RESEARCH BACKGROUND 4
2.1 Cancer 4
2.2 Biomedical Applications of Nanocarriers 5
2.2.1 Polymersome Nanocarriers 8
2.2.2 Development of Multimodal Polymersomes 10
2.3 Biomedical Applications of Magnetic Nanoparticles 11
2.3.1 Properties of Superparamagnetic Iron Oxide Nanoparticles . . . 17
2.3.2 Synthesis and Surface Coating of Superparamagnetic Iron Oxide Nanoparticles 19
2.4 Cyclodextrins (CDs) 22
2.4.1 The Chemistry of Cyclodextrins: Structure, Properties, and Complexation 22
2.4.2 β-Cyclodextrins 25
2.5 Design of SPION-Interacted Polymersomes 28
2.5.1 Polyethylene Glycol 29
2.5.2 2-(Diethylamino)ethyl Methacrylate 30
2.5.3 Ferrocene 31

2.5.4 Cross-Linkers . . . 33
3. METHODS . . . 34
3.1 Materials . . . 34
3.2 Methods . . . 35
3.2.1 Synthesis of β-CD Coated Superparamagnetic Iron Oxide Nanoparticles . . . 35
3.2.2 Characterization of β-CD Coated Suparparamagnetic Iron Oxide Nanoparticles . . . 37
3.2.2.1 Solid Content Analysis . . . 37
3.2.2.2 Size and Polydispersity Index Measurement . . . 37
3.2.2.3 Morphological Characterization . . . 38
3.2.2.4 Vibrating-Sample Magnetometer . . . 38
3.2.2.5 Fourier-Transform Infrared Spectroscopy . . . 39
3.2.2.6 Thermogravimetric Analysis . . . 39
3.2.2.7 Investigation of SPIONs' pH Sensitivity . . . 39
3.2.2.8 Time-Dependent Stability Assessment of β-CD coated SPION . . . 40
3.2.3 Preparation of Polymersomes . . . 40
3.2.3.1 Preparation of Ferrocene-Free Polymersomes . . . 40
3.2.3.2 Preparation of Ferrocene-Containing Polymersome . . . 41
3.2.4 Characterization of Polymersomes . . . 41
3.2.4.1 Size and Polydispersity Index Measurement . . . 42
3.2.4.2 Morphological Characterization . . . 42
3.2.5 Interaction Between SPIONs and Polymersomes . . . 42
3.2.6 Characterization Study on SPION-Polymersome Interactions . . . 43
3.2.6.1 Size and Polydispersity Index Measurement . . . 43
3.2.6.2 Morphological Characterization . . . 43
4. RESULTS and DISCUSSION . . . 44
4.1 Characterization Results of β-CD Coated Superparamagnetic Iron Oxide Nanoparticles . . . 44
4.1.1 Solid Content Analysis . . . 44
4.1.2 Size and Polydispersity Index Measurement . . . 44

4.1.3 Morphological Characterization 45
4.1.4 Vibrating-Sample Magnetometer 47
4.1.5 Fourier-Transform Infrared Spectroscopy 48
4.1.6 Thermogravimetric Analysis 49
4.1.7 Investigation of SPIONs' pH Sensitivity 50
4.1.8 Phosphate Buffered Saline (PBS)-Based pH Optimization 52
4.1.9 Time-Dependent Stability Assessment of β-CD coated SPIONs . 53
4.2 Characterization Results of Polymersomes 54
4.2.1 Size and Polydispersity Index Measurement 54
4.2.1.1 Preparation of Ferrocene-Free Polymersomes 54
4.2.1.2 Preparation of Ferrocene-Containing Polymersome . . 55
4.2.2 Morphological Characterization 57
4.3 Characterization Results of SPION-Polymersome Interactions 58
4.3.1 Size and Polydispersity Index Measurement 58
4.3.2 Morphological Characterization 60
5. CONCLUSIONS AND OUTLOOK 62
5.1 Conclusions 62
5.2 Future Directions in Research 64
REFERENCES 65

LIST OF FIGURES

2.1	Overview of Nanocarriers in Biomedical Applications [19].	6
2.2	A schematic representation of the polymer nanoparticles [24].	7
2.3	A schematic representation of the polymersome [30].	8
2.4	The Role of Magnetic Nanoparticles in Biomedical Applications [47].	12
2.5	The Role of Magnetic Nanoparticles in Biomedical Applications [55].	14
2.6	Diagram illustrating the different methods used in the synthesis of Magnetic Nanoparticles.	15
2.7	The crystal structures and crystallographic information of hematite, magnetite, and maghemite are illustrated (with Fe^{2+} depicted as a black ball, Fe^{3+} as a green ball, and $O^{2}-$ as a red ball) [66].	18
2.8	Color transformation in SPIONs synthesis via co-precipitation: From yellow to black [69].	19
2.9	Schematic Illustration of β-Cyclodextrin Coated SPION.	21
2.10	Structure of cyclodextrins [80].	23
2.11	Properties of cyclodextrins [81].	23
2.12	Schematic representation of an optimal host-guest interaction in cyclodextrin-based systems.	24
2.13	Chemical structure of β-Cyclodextrin [79].	26
2.14	Schematic illustration of the key features of β-Cyclodextrin.	27
2.15	Schematic illustration of interaction between β-CD and Ferrocene units.	29
2.16	The repeating unit of the Polyethylene Glycol chain.	29
2.17	Chemical structure of DEAEMA.	31
2.18	Chemical structure of Ferrocene.	32
2.19	Chemical structure of FcMA [97].	32
3.1	The formation of SPIONs following the addition of NH_4OH.	35
3.2	Dried ferrophase sample after the 24-hour drying process.	36

3.3	β-CD coated SPIONs.	36
3.4	Ferrocene-Containing Polymersome.	41
4.1	TEM Images of β-CD Coated SPIONs at 1mg/mL concentration, presented at 100 nm scale.	46
4.2	TEM Images of the supernatant phase of β-CD Coated SPIONs, at 100 nm Scale.	46
4.3	VSM analysis of Bare SPIONs and β-CD coated SPIONs.	47
4.4	FTIR spectra of Bare SPIONs, β-CD, and β-CD coated SPIONs.	48
4.5	TGA Analysis of Bare SPIONs and β-CD Coated SPIONs.	50
4.6	pH Alteration Study of β-CD Coated SPIONs Samples: (a) Sample with 1 mg/mL concentration; (b) Supernatant sample.	51
4.7	Visual Representation of Aggregation in β-CD coated SPIONs at pH 6.05.	52
4.8	DLS Measurements of Ferrocene-Free Polymersomes Produced from BCP1.	55
4.9	pH Cycle Study of FFP Produced from BCP1.	56
4.10	DLS Measurements of FCP Produced from BCP2.	56
4.11	pH Cycle Study of Ferrocene Containing Polymersomes Produced from BCP2.	57
4.12	a) STEM image of Empty Ferrocene-Free Polymersome at a 50 nm scale. b) STEM image of Empty Ferrocene-Containing Polymersome at a 500 nm scale.	57
4.13	STEM analysis of SPION-Interacted Ferrocene-Containing Polymersome.	60
4.14	STEM Analysis of Re-dispersed Ferrocene-Containing Polymersome' Pellet After Centrifugation.	61

LIST OF TABLES

2.1	Spin alignment patterns	13
2.2	Summary of Methods for MNP Production	16
3.1	Detailed Compositions of the Block Copolymers	34
4.1	Hydrodynamic Size and PDI of Synthesized β-CD coated SPIONs	45
4.2	Hydrodynamic Size and PDI of the β-CD coated SPIONs in PBS	53
4.3	Time-Dependent Stability of Hydrodynamic Size and PdI for β-CD Coated SPIONs	53
4.4	Hydrodynamic Size and PdI of the Ferrocene-Free Polymersome (FFP) interacting with the β-CD coated SPIONs	59
4.5	Hydrodynamic Size and PdI of the Ferrocene-Containing Polymersome (FCP) interacting with the β-CD coated SPIONs	59

LIST OF SYMBOLS

%	Percentage
%wt	Weight Percent
°	Degree
°C	Celcius
g	Gram
μg	Microgram
μl	Microliter
kDa	Kilodalton
kV	Kilovolt
M	Molar
m^2	Square Meter
mg	Milligram
mL	Milliliter
mM	Millimolar
nm	Nanometer
rpm	Revolution per Minute

LIST OF ABBREVIATIONS

BCP	Block Copolymer
β-CD	β-Cyclodextrin
DMIBMA	3,4-dimethyl maleic imidobutyl methacrylate
DMIHMA	3,4-dimethyl maleic imidohexyl methacrylate
DMAEMA	2-(Dimethylamino)ethyl Methacrylate
DLS	Dynamic Light Scattering
DOX	Doxorubicin
FCP	Ferrocene-Containing Polymersomes
FcMA	2-(methylacryloyloxy)ethyl ferrocencarboxylate
FDA	Food and Drug Administration
FFP	Ferrocene-Free Polymersomes
FTIR	Fourier Transform Infrared Spectroscopy
H_2O	Water
MNPs	Magnetic Nanoparticles
MRI	Magnetic Resonance Imaging
NP	Nanoparticle
PBS	Phosphate Buffered Saline
PdI	Polydispersity Index
PEG	Polyethylene Glycol
STEM	Scanning Transmission Electron Microscopy
SPION	Superparamagnetic Iron Oxide Nanoparticles
TGA	Thermogravimetric Analysis
THF	Tetrahydrofuran
TEM	Transmission Electron Microscopy
VSM	Vibrating-Sample Magnetometer

1. INTRODUCTION

1.1 Motivation and Aim

According to the 2020 data from the International Cancer Research Agency, 19.3 million new instances of cancer and 10 million deaths due to cancer occured, around the globe. [1]. When it comes to the treatment of cancer; surgery, radiation, and chemotherapy are among the most frequently applied treatment options by doctors. The types of treatment a patient will receive are determined by the type of cancer and its stage. Surgery is the most effective method of treating cancer, but it can only be applied to patients in the early stages. Radiotherapy can be used in the treatment of early-stage cancer patients who are not suitable for surgical operations. Chemotherapy provides benefits over radiation and surgery in the treatment of locally advanced or metastasized cancer, however, serious toxicities caused by chemotherapeutic drugs limit their use [2].

Targeted therapy is a treatment modality in which drugs or other substances are used to accurately identify and attack specific cancer cells [3]. This approach has several advantages, including reducing toxic effects, minimizing drug resistance mechanisms by targeting different action mechanisms, reducing tumor growth, and increasing clinical response through synergy or additive effect [4]. Current studies show that magnetic nanoparticles (MNPs) are suitable for targeted therapy due to their specific magnetic properties [5]. In addition, drug targeting with MNPs is a promising method for delivering drugs to tumors with low side effects [6]. However, the drug targeting with MNPs lacks the capacity for precise localization of abnormal tissue or targeted cells. It is critical to release drugs just in specific parts of the body to improve therapeutic efficiency and prevent side effects. Although the strategy of drug targeting with MNPs was suggested more than 30 years ago, the effectiveness of magnetic drug targeting must be enhanced mainly by the external triggering of specific enzymes in the target site, pH changes, light, ultrasound, or magnetic field stimuli [7].

In this study, a multimodal nanocarrier system that responds to pH stimuli will be developed with magnetic nanoparticles. The development of such a multimodal system will provide several therapeutic advantages. For one, targeting with both a magnetic field and pH can improve the influence drug's efficacy in tumor tissue. Tumor tissues are acidic in comparison to normal tissues [8]; since the pH-sensitive system will release chemotherapy drugs in an acidic environment, targeted delivery will be more effective. In addition, real-time data can be obtained with this multimodal system designed with magnetic nanoparticles. This method provides for a significant reduction in chemotherapy-related side effects.

1.2 Objectives

The primary objective of this thesis is to design a pH-sensitive polymeric nanocarrier system that interacts with superparamagnetic iron oxide nanoparticles (SPIONs) for use in potential applications. The synthesized polymer blocks form a spherical nanocarrier system under alkaline pH conditions, while the system grows in size under acidic pH conditions to form openings and can release the encapsulated material in a controlled manner.

To achieve this ultimate objective, the following studies were carried out:

Objective-1: SPIONs were produced via the co-precipitation method from an aqueous Fe3+/Fe2+ solution (ratio 2:1) using concentrated ammonium hydroxide in excess. The nanoparticles were subsequently coated with β-Cyclodextrin (β-CD) to enable their dispersion in an aqueous solution.

Objective-2: A variety of characterization methods were used to describe β-CD coated SPIONs physicochemical and morphological characteristics.

Objective-3: Biocompatible polymersomes were generated where Poly(ethylene glycol) (PEG) was the hydrophilic part of the amphiphilic block copolymer, and 2-

(diethylamino)ethyl methacrylate (DEAEM), photo cross-linker groups and Ferrocene segments formed together with the hydrophobic part. A similar polymersome, which did not contain the Ferrocene segments but contained PEG, DEAME, and crosslinker, was produced as a control group.

Objective-4: Different characterization methods were used to characterize polymersomes' physicochemical and morphological characteristics.

Objective-5: For the purpose of promoting surface interaction and direct interactions between both components, polymersomes have been kept in a controlled environment with β-CD coated SPIONs.

Objective-6: Various analysis methods were used to characterize the structure of β-CD coated SPION interacted polymersomes.

1.3 Thesis Outline

Background Information is presented in Chapter 2; firstly a brief overview regarding cancer, which is a major theme of the study is provided, it is followed by an extensive discussion of nanocarriers, magnetic nanoparticles, and cyclodextrins in detail. Chapter 3 provides explanations of the materials and methods used in this study. The methods are described in six subsections. These subsections include the synthesis and characterization of β-CD coated SPIONs, the generation and characterization of polymersomes, and finally the interaction of β-CD coated SPIONs with polymersomes and their characterization. All the results and discussion of experiments are set out in Chapter 4. Finally, the conclusions, the outlook, and the future approach to research are described in Chapter 5.

2. RESEARCH BACKGROUND

2.1 Cancer

Cancer has a significant impact on global death rates and has a considerable effect on public health and life expectancy worldwide. According to data from throughout the world in 2020, there were 19.3 million instances of new cancer diagnoses and 10 million mortalities related to cancer [1]. This demonstrates how cancer is a serious worldwide health issue that continues to overwhelm healthcare systems and substantially reduces biological lifetime.

Cancer is a very complex disease, identified by uncontrolled division and cell proliferation which significantly impairs the function of healthy cells [8]. In order to be effective in the treatment of cancer and to improve the overall survival of patients, early diagnosis is essential. Unfortunately, only about half of the cancer cases can be detected at an advanced stage [9].

Surgery, radiotherapy and chemotherapy are the main types of cancer treatment employed in today's practice. The main role in determining the treatment protocol is played by the type and stage of the cancer. In early stage cancers, surgery is generally preferred and is highly effective in cases where the disease can be completely removed. However, microscopic tumor cells are always at risk of remaining in the surgical site, which may lead to recurrence of the disease in the future, due to the nature of the surgical procedure [10]. In the case where surgery is not suitable, radiotherapy provides a good option for treatment. However, it also has the potential to damage healthy cells in the affected location, leading to burns on the skin, fatigue and other adverse effects [11]. Although chemotherapy is a common treatment, it significantly impacts patients' quality of life due to its high toxicity and numerous side effects. [12]. Based on the possible limitations and adverse effects of these treatments, further development and improvement in cancer treatment is required. New treatment methods with a

higher degree of efficiency and lower side effects than current treatments are always the main objective, owing to advances in technology and scientific discoveries.

2.2 Biomedical Applications of Nanocarriers

Nanotechnology represents the science of constructing minuscule instruments by modifying entities at their atomic or molecular constituents. This idea was initially proposed by Richard P. Feynman during his memorable lecture at Caltech in 1959, "There's Plenty of Room at the Bottom", where he speculated about the prospects of altering materials at their atomic and molecular dimensions [13]. Norio Taniguchi further expounded upon this definition in 1974, characterizing nanotechnology as "the operation of dividing, amalgamating, and reshaping materials at the level of a single atom or molecule" [14]. From the 1990s, nanotechnology has demonstrated expansive potential, with a significant impact on the emergence of nanomedicine over recent decades. This innovative scientific field is devoted to the diagnosis, treatment, and prevention of diseases [15]. Nanomedicine has made remarkable advancements, particularly in cancer detection and treatment, employing imaging technologies. Even for those seemingly healthy, periodic screenings - notably for cancers like cervical, breast, colorectal, thyroid, and prostate - are paramount for early detection and intervention, thereby enhancing the likelihood of successful outcomes [16].

Biomedical engineering, a pivotal catalyst propelling advancements across a multitude of sectors, has staked its claim in the landscape of pharmaceutical industry and effective drug design in the 21st century [17]. A key focus in this area is the targeted drug delivery, a method that ensures the drug molecules interacts only within the affected area [18]. This is described as the propensity of a drug's active component to concentrate in the desired tissue or organ, irrespective of its chemical composition and absorption [19]. The deployment of assorted targeted nanocarriers has become a cornerstone in the realm of biotechnological pharmaceutical technologies. These nanocarriers are diminutive structures capable of carrying a diverse range of medicinal substances and/or imaging compounds. For that matter, these various nanocarriers serve a vital

part in the advancement of better and more efficient healthcare applications. As seen in Figure 2.1., there are various types of nanocarriers available.

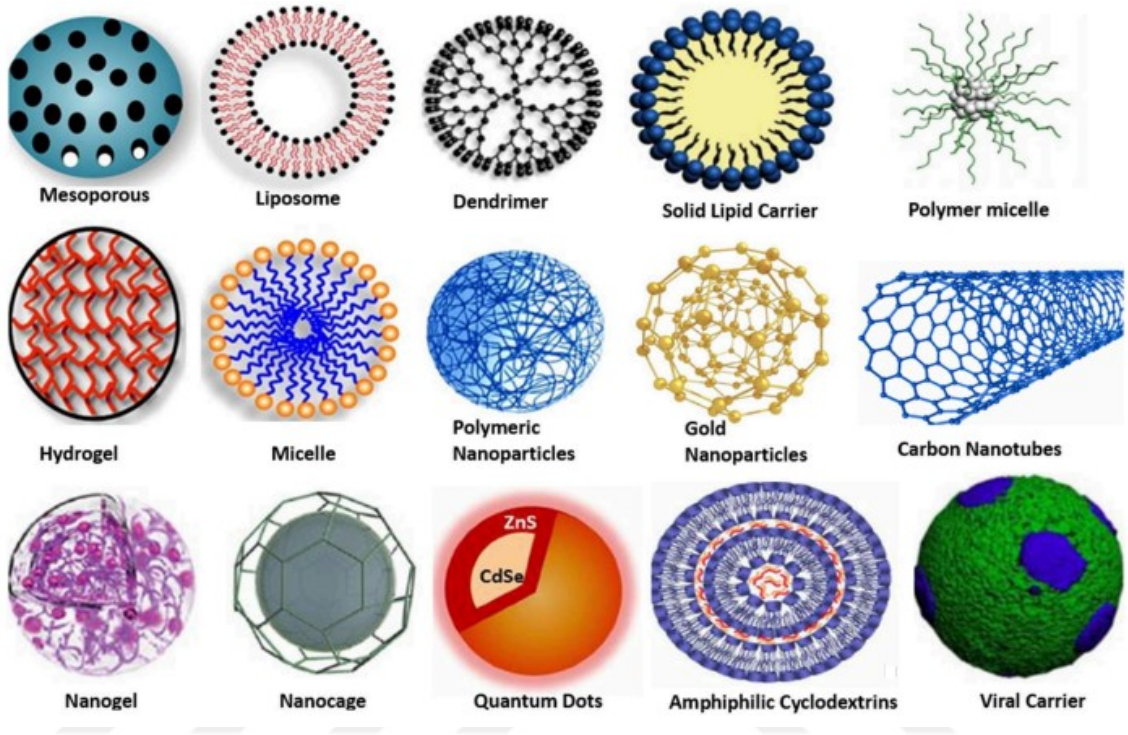

Figure 2.1. Overview of Nanocarriers in Biomedical Applications [19].

Polymer nanoparticles, which have led to significant interest in pharmaceutical and medical technologies over the last years, are most commonly employed as drug delivery systems [20].Figure 2.2 shows the schematic representation of the sketch polymer nanoparticles. These nanoparticles are typically manufactured by chemical or physical processes, which may be different depending on the polymer and drug chosen [21]. As an example, biodegradable and water soluble polymers are frequently treated by techniques such as emulsification [22].

Polymer nanocarriers can be classified as nanospheres or nanocapsules based on their morphology [20] [23]. These nanocarriers aim to enhance the effectiveness of drugs by leveraging the unique properties of polymers The drug can be conjugated to nanospheres, which are typically homogeneous matrix systems wherein the drug is dispersed throughout the material [21]. Alternatively, the drug can be adsorbed in the pores or on the surface of these particles. In addition, nanocapsules can be divided into

two parts: the core and the shell [19]. Depending on the type of use, the core material may be solids, liquids or gases. The shell is composed of polymeric materials in most cases.In general, the drug is found in the core part, while the shell protects them from the external surroundings. Moreover, the ability to integrate different materials into their shell and adsorb substances onto their surface broadens their utility, potentially enabling the simultaneous delivery of one or more therapeutic agents.

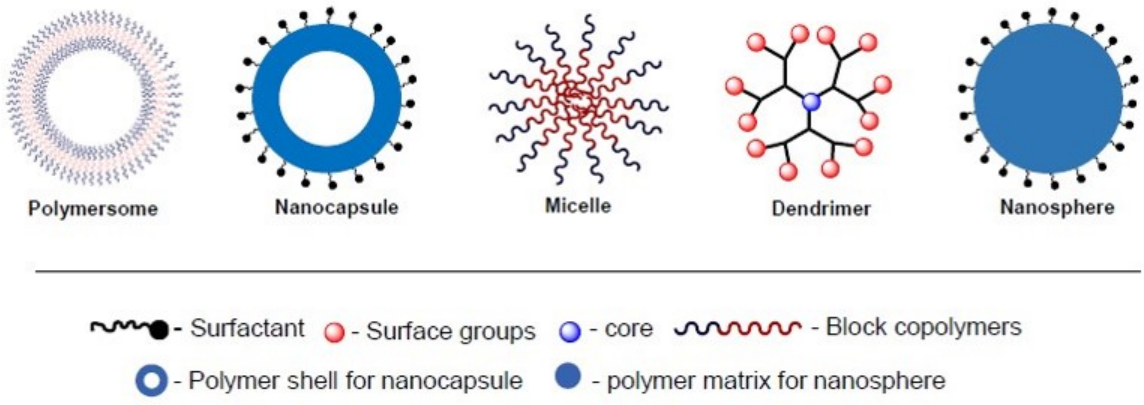

Figure 2.2. A schematic representation of the polymer nanoparticles [24].

Polymer nanocarriers have a wide range of beneficial features, including biocompatibility, biodegradability, surface adaptability and ease of functionalization [25]. The biocompatibility of the polymer nanocarriers makes it easier for them to interact well with cells and tissues in the body, reducing side effects on the whole system [21]. The biodegradability of the nanocapsules ensures that when the medicine reaches the target area, they safely dissolve and disintegrate [26]. Furthermore, their surface modifiability enables the synthesis of customized drug delivery systems which can be modified with different molecules or drugs. These characteristics give polymers nanocarriers the potential to become a breakthrough technology in targeted drug delivery.

2.2.1 Polymersome Nanocarriers

Polymersomes are polymer vesicles that self-assembly from an assortment of synthetic amphiphilic block copolymers, which are composed of both hydrophilic and hydrophobic segments [27] [28]. These nanostructures, first described by Discher et al. in 1999 [29], form a polymeric membrane that surrounds the aqueous lumen. The membrane structure primarily consists of the copolymer's hydrophobic block, designed to reduce contact with the aqueous medium, while its hydrophilic counterpart projects into both the lumen of the polymersome and the external aqueous environment. Due to their compatibility with various chemical modifications, polymersomes are incredibly versatile, allowing them to serve different purposes.

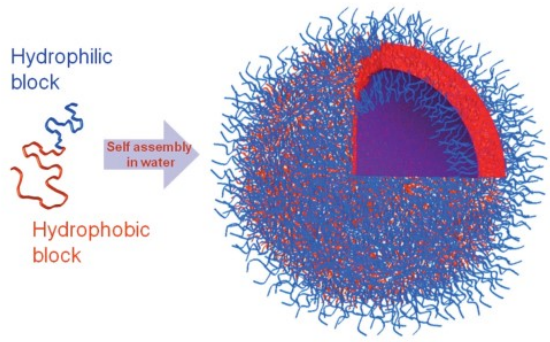

Figure 2.3. A schematic representation of the polymersome [30].

Block copolymers, which are known for their amphiphilic properties, are used for the production of polymersomes [31]. Block copolymers are complex macro molecules composed of chemically diverse monomer blocks arranged in a specific sequence [32]. In the composition or sequence distribution of those monomers, there may be variations. If a block copolymer has both hydrophobic (non-polar) and hydrophilic (polar) blocks, it exhibits amphiphilic attributes. These amphiphilic block copolymers exhibit a tendency for self-assembly with a variety of molecular structures, including micelles, rods, or polymersomes in aqueous solution [33]. The ability of those block copolymers to form such structures is a significant feature, given that their hydrophilic and hydrophobic segments are balanced. These structures offer promising platforms for the delivery of drugs, imaging and other biomedical applications as well as their ability to encapsulate molecules of interest.

Polymersome production involves numerous techniques, generally falling into two primary categories. The first method is known as "top-down", where vesicles are formed from a large amount of amphiphilic block copolymers [34]. The second category is the "bottom-up" approach, which involves the formation of vesicles from unimers or monomers, which are then polymerised into amphiphilic copolymers in a selective solvent for a single block, leading to the formation of vesicles [34].

Latest and innovative techniques for the preparation of polymers include electrohydration, rehydration, microfluidics, emulsion phase transfer, direct injection of polymers, and polymerization-induced self-assembly (PISA) [35]. Electrohydration [29] [36], a method whereby the electrolyte is used to form vesicles and film rehydration [37], which entails hydration of dry lipid films in order to form vesicles. The ease and affordability of film rehydration is the factor that makes this easy and inexpensive process popular. Microfluidics, which is regarded as the most recent breakthrough in this area, provides nearly complete control of polymersome formation and size distribution [38] [39]. Emulsion phase transfer adds more control to the direct injection method, producing homogeneous and uniform vesicle sizes [40]. The most frequently used method of solvent displacement is direct injection, which uses a polymer's solubility differences between organic solvents and aqueous solutions [41]. Lastly,the PISA uses differences in the solubility of monomers and polymers [42]. It can also activate the self assembling of block copolymers to polymersomes with a change in stimuli like pH or temperature [43]. These methods provide a wide range of possibilities for control and precise manufacture of polymers.

Each method of polymersome production has its own unique advantages and drawbacks. The characteristics of the resulting polymersome may be significantly influenced by the choice of method. For instance, selected method may affect their size, stability and ability to contain other molecules that in turn has an impact on whether such substances are used for applications like drug delivery or imaging.

2.2.2 Development of Multimodal Polymersomes

As regards drug delivery systems and biomedical applications, multimodal polymersomes represent a new frontier for nanotechnology. These self-assembled structures consist of amphiphilic block copolymers, and in the structure of their double layer membrane they are able to encapsulate both hydrophilic and hydrophobic drugs simultaneously [24]. Multimodal polymersomes constitute promising systems for the targeted delivery of therapeutic drugs and response mechanisms, providing greater stability and encapsulation versatility compared to liposomes. The potential for these multifunctional nanocarriers to transform the biomedical sector is only going to grow as researchers continue their exploration of polymer science's dynamic world.

Innovative polymersomes have been ingeniously designed to incorporate responsive elements that can alter the release of an encapsulated payload, and they are called "smart" for their ability to penetrate complex biological barriers.These components provide the capacity for these polymersomes to adjust to particular environmental cues or shifts in bodily parameters like variations in pH, redox conditions, and temperature, or the presence of externally applied stimuli [44]. This flexibility significantly enhances their potential applications and makes them more efficient in a wide variety of treatment scenarios, which is leading to a new era for biomedical products.

Systems that respond to pH are a significant class of multimodal polymersomes. Extracellular acidity is known to be highly correlated with pathological conditions including cancer and inflammation, which makes pH-responsive drug delivery systems extremely useful in medical applications [44]. In parallel, magnetic-driven drug delivery is another promising area. The potential for targeting and controlling drug delivery can be achieved through strategies involving Superparamagnetic Iron Oxide Nanoparticles (SPIONS) in polymersomes.Although there are many different types of inorganic magnetic nanoparticles available, SPIONs are preferred because they are biodegradable and non-toxic and since the iron component can be reused or metabolized by cells through regular biochemical metabolic pathways [45]. In the field of multimodal drug delivery, the potential of such systems is enormous, promising the development

of efficient therapeutic tools.

Building upon this existing knowledge, our research has focused on the production of Beta-Cyclodextrin (β-CD) coated SPIONs contained within a pH-responsive polymersome. This development represents an important step towards a multimodal and smart drug delivery system that can react to pH changes, guided by magnetic fields which may also provide additional functionality via the use of β-CD.

2.3 Biomedical Applications of Magnetic Nanoparticles

Magnetic nanoparticles (MNPs), with sizes between 1 and 100 nm, are used in a wide range of therapeutic and diagnostic procedures in the biomedical applications [46]. The use of MNPs provides a very innovative approach to the treatment and diagnosis of diseases. MNPs applications have quickly expanded in the biomedical area, especially in fields like drug delivery, hyperthermia, tissue engineering, theragnosis, bioseparation, and manipulation. [47].

Figure 2.4 provides a schematic representation of the general usage areas of MNPs. Consequently, the ability of these materials to interact with biological systems constitutes a key element in development of High Technology Therapeutic and Diagnostic Methods. Moreover, it is possible to develop new applications in these areas by virtue of high surface-to-area ratios for nanoparticles and their interaction with biological systems.

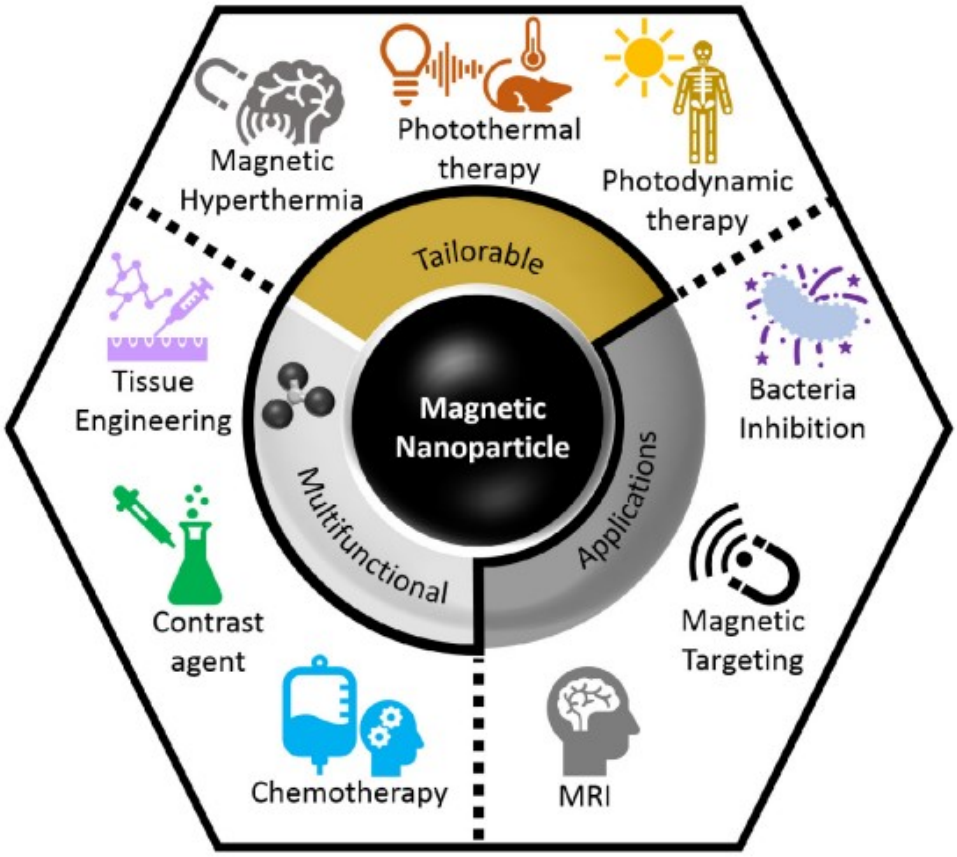

Figure 2.4. The Role of Magnetic Nanoparticles in Biomedical Applications [47].

There is a generally random orientation of magnetic dipole moments in unmagnetised materials. Nonetheless, these moments are prone to align themselves in relation to the orientation of the application field when such material is exposed to an electromagnetic field. The materials can be classified into a number of groups such as diamagnetic, paramagnetic, ferromagnetic or superparamagnetic depending on how they are responding to the magnetic field [48]. Different types of materials, including diamagnetism, paramagnetism, ferromagnetism and superparamagnetism, show different spin alignment patterns due to external magnetic fields as summarised in Table 2.1.

Table 2.1. Spin alignment patterns

Material Type	**Spin Alignment**
Diamagnetic	Random, but tends to align oppositely in an external magnetic field
Paramagnetic	Random, but aligns parallelly in an external magnetic field
Ferromagnetic	Parallel alignment in domains, remains aligned even without an external magnetic field
Superparamagnetic	Random, but can align strongly in an external magnetic field, returns to randomness when the field is removed

The diamagnetic material, due to changes in its electron orbital motion caused by the applied field, produces an opposing magnetization when exposed to a magnetic field [49]. This accelerates electron orbits, and in doing so changes the magnetic dipole moment within the substance, which results in a molecular magnetic field that opposes an external one. Under specific circumstances, such as changes in temperature, ferromagnetic elements, become permanent magnets or are magnetically attracted [50]. Due to the alignment of their atomic magnetic moments, they remain magnetic even after the external field has been removed. On the other hand, a paramagnetism material is aligned with an External magnetic field but does not retain magnetism once it has been taken out [51]. The superparamagnetic material, as a subtype of paramagnets, has high magnetism under the magnetic field that is similar to ferro magnets but switches back to an unmagnetic state once it's removed [52].

Due to their high surface-to-volume ratio and size-dependent magnetic characteristics, MNPs have special qualities that aren't found in their bulk equivalents [46] [53]. The specific characteristics give rise to an extremely high level of strength, reactivity and adaptability. The fact that magnetic nanoparticles exhibit superparamagnetic properties due to their nanoscale dimensions is a key characteristic of this situation [54].

As shown in Figure 2.5, Magnetic nanoparticles (MNPs) are typically made up of magnetic elements like iron, cobalt, nickel, and their corresponding alloys. These elements have properties such as ferromagnetism and superparamagnetism [55]. More specifically, due to their ability to direct and control at the target sites of treatment, its superparamagnetic properties substantially increase the potential for use of MNPs on biomedical applications.The surface chemistry of MNPs must be considered to prevent

their agglomeration. They should be stabilized with a variety of materials, including organic and inorganic coatings [56]. For biomedical applications, it is critical that these magnetic nanoparticles remain stable in water at a pH of approximately 7 and salinity levels close to physiological norms. Therefore, to enhance their performance and stability, MNPs are frequently covered with a layer of ceramics, polymers, or highly charged/sterically hindered molecules [47].

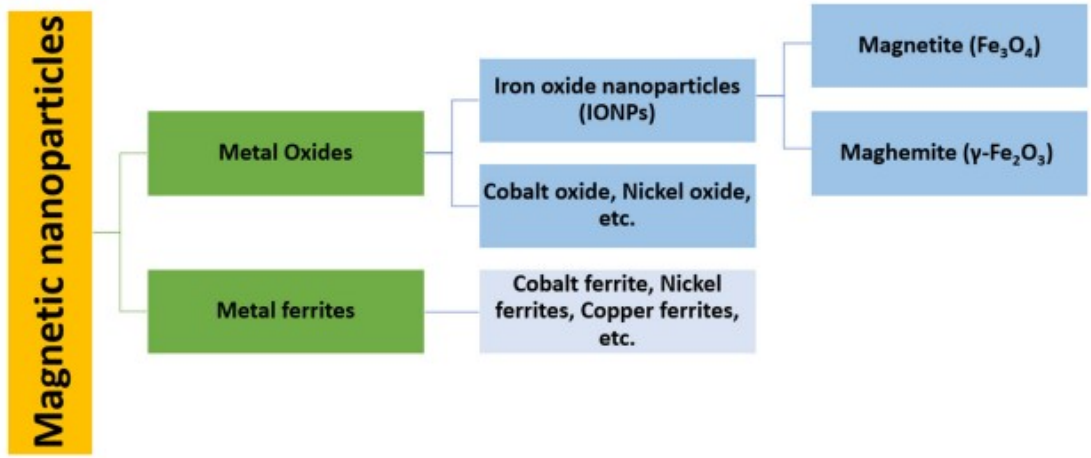

Figure 2.5. The Role of Magnetic Nanoparticles in Biomedical Applications [55].

In the current scientific landscape, a multitude of strategies have been devised for the construction of MNPs, with the primary methodologies falling into two categories: top-down and bottom-up approaches [57]. Top-down is the method of breaking a magnetic sample to its nanoscale size, such as high energy ball milling. The ability of the technique to produce large volumes of particles by a single batch is one of its advantages [46]. However, the control over particle size and shape is often compromised which has a major impact on biomedical applications.

By contrast, the "bottom up" approach consists of nanoforming or synthesising nanoparticles made from either atom or molecular elements that results in greater control over particle size and morphology [58]. Both of these strategies have an integral role to play in the field of nanotechnologies, each having its unique advantages and disadvantages. Various chemical methods have been established to synthesize MNPs, including co-precipitation, thermal decomposition, microemulsion, sol-gel, polyol, and hydrothermal methods [55] [57]. These techniques are illustrated in Figure 2.6. These

strategies allow for control of the size, shape and composition of microplastics while at the same time being cost effective. Various methods can be employed to produce nanoparticles of diverse sizes and forms such as spheres, pallets, nanorods, nanotubes or many more.

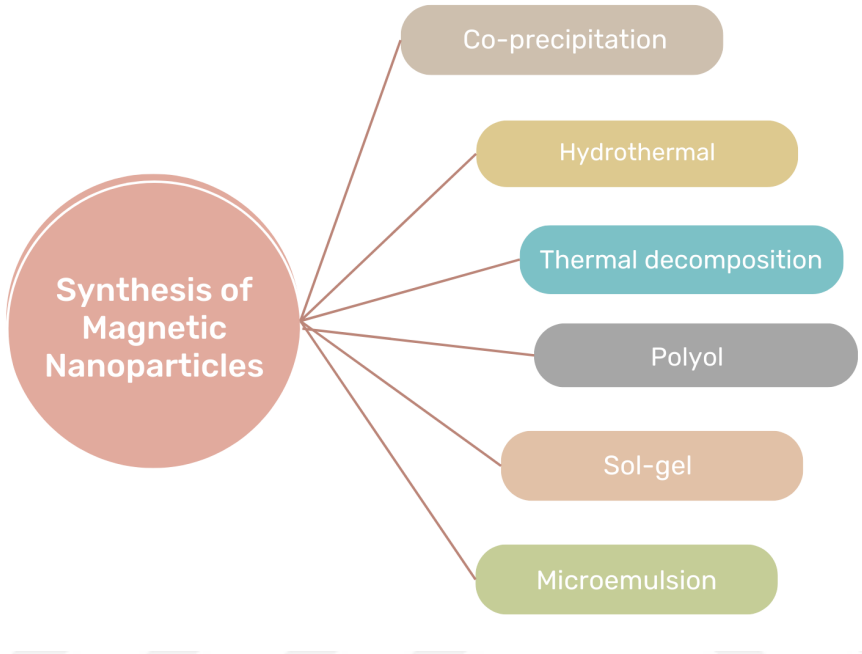

Figure 2.6. Diagram illustrating the different methods used in the synthesis of Magnetic Nanoparticles.

A comprehensive overview of the various approaches employed for the production of MNPs is presented in Table 2.2. Their unique processes and their characteristics for the production of nanoparticles have been taken into account to classify these methods.

Table 2.2. Summary of Methods for MNP Production

Method	Description
Co-precipitation	It is commonly used in biomedical applications for reasons of safety, cost effectiveness and low synthesis temperature. It involves precipitation of one or more substances, often starting with a 2:1 ratio of ferrous and ferric salt under basic conditions [57].
Hydrothermal	It is used for the crystallisation of an enclosed container using wet chemical techniques. The aqueous solution shall be kept in a container at high temperature and pressure, most commonly resulting in larger diameter MNPs [59].
Thermal Decomposition	This involves heating premix materials, solvents and surfactants within a specific temperature range which offers fine tuning of particle diameter [60].
Polyol	It is composed of a liquid polyol, which acts as a solvent for the metallic precursors, reduction agents and sometimes complexing agents to cations. Nanoparticle size may be controlled through heterogeneous nucleation [61].
Sol-gel	Involves the production of MNPs through a condensation and hydrolysis reaction between metal alkoxides or their precursors. The precursors dissolve into the water, then a series of stirs and heating steps are taken. In order to form a gel, the MNPs are dried [55].
Microemulsion	It involves the use of isotropic liquid mixtures of oil, water and surfactants, which are thermodynamically stable. This method produces larger MNPs in size and requires the use of a high temperature to synthesise them [57].

2.3.1 Properties of Superparamagnetic Iron Oxide Nanoparticles

Over recent years, notable progress has been made in the realm of nanotechnology, particularly within the biomedical industries. SPIONs, the only clinically approved metal oxide nanoparticles, stand out among the broad range of available nanoparticles due to their unique magnetic properties [62]. This distinctive feature makes it possible to apply in many fields of medicine a wide range of innovative applications.

SPIONs are highly desirable for medical applications due to their decreased toxicity and a very high density of the surface area compared to volume ratio, as well as being easy to separate by using magnetic fields [63]. Their immense potential is displayed by applications such as magnetic resonance imaging (MRI), targeted delivery of medicinal products or genes, tissue engineering, targeting the destruction of tumor tissues via hyperthermia, magnetic transfections, iron detection and chelation therapy, and other areas of tissue engineering. [64]. However, there is still a need to explore their potential for medicinal use. An interesting area of research is the possibility to use magnetic properties of SPIONs for targeted drug delivery, but it currently requires extensive exploration and experimentation.

In the different biological phenomena, SPIONs play a vital role owing to their easy availability, affordability or flexibility. These nanoparticles are small synthetic particles, mainly composed of maghemite($\gamma-Fe_2O_3$), magnetite (Fe_3O_4) or hematite ($\alpha-Fe_2O_3$) as illustrated in Figure 2.7. Its core diameter is usually in the 10 to 100 nm range [65]. Extensive use has been achieved in a number of medical applications, particularly for magnetite and maghemite nanoparticles.

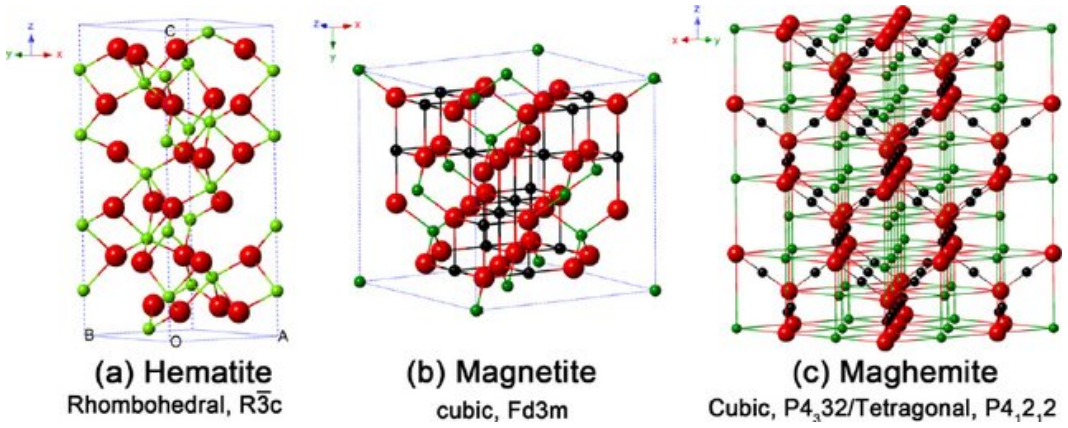

Figure 2.7. The crystal structures and crystallographic information of hematite, magnetite, and maghemite are illustrated (with Fe^{2+} depicted as a black ball, Fe^{3+} as a green ball, and $O^{2}-$ as a red ball) [66].

The SPIONs have a special property called "superparamagnetism." They are magnetized up to their saturation magnetization limit in the presence of an external magnetic field. Once the magnetic field is removed, they cease to exhibit any remaining magnetic interaction. This trait is size-dependent, generally appearing when the nanoparticle size drops to as low as 10-20 nm [65]. Additionally, SPIONs do not have the multiple domains as seen in larger magnets at this small size. Instead, they've become a single magnetic field with high magnetic susceptibility and behave like "one super spin" [67]. Consequently, these nanoparticles have a faster and more powerful magnetic response than their larger counterparts, with virtually no remanence or coercivity, when subjected to a magnetic field. This superparamagnetism, which is exclusive to nanoparticles, is especially important in terms of their role as drug delivery vehicles. In theory,under the application of a magnetic field, these nanoparticles have the ability to "pull" drug molecules towards specific target sites within the body.

Another advantage is that these particles do not have any remaining magnetism at room temperature after removal of the magnet field, which reduces the likelihood of aggregation. This feature makes it easy to dispersion, reduces phagocytic uptake, and prolongs the length of circulation [65]. Furthermore, their low agglomerativity makes the SPIONs relatively unlikely to cause thrombosis or blockage of blood capillaries, and thus contribute to its safety profile for medical use [65]. As a result, these nanoparticles

are essential to the improvement of biomedical research and applications in the future.

2.3.2 Synthesis and Surface Coating of Superparamagnetic Iron Oxide Nanoparticles

Generally, as shown in Figure 2.8, co-precipitation is the preferred method to produce a homogenous iron based nanoparticles in an aqueous solution. In the co-precipitation method for the synthesis of SPIONs, a base is incorporated into an aqueous solution. The solution consists of a measured mixture of ferrous Fe^{2+} and ferric Fe^{3+} ions, in accordance with a 1:2 stoichiometry, all in an oxygen free environment [68]. This approach will result in the formation of SPIONs that are characterized by a dark magnetic nanoparticles. In particular, the average diameter of these nanoparticles is approximately 20 nm, which is considered to be very ideal for a variety of medicinal applications.

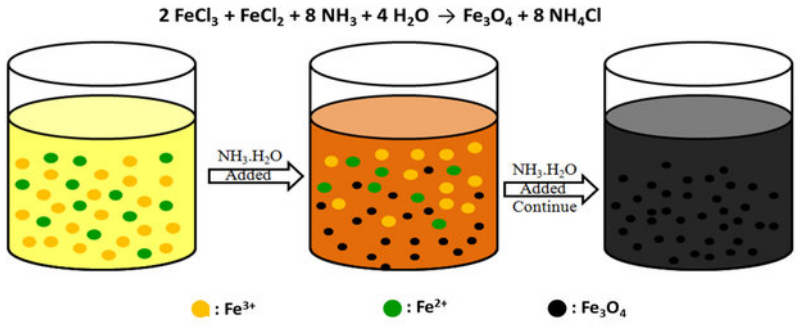

Figure 2.8. Color transformation in SPIONs synthesis via co-precipitation: From yellow to black [69].

The pH and ionic strength of the solution used for precipitation considerably impact the size of MNPs produced via co-precipitation. The increased pH and ionic strength of the medium is determined to lead to a reduction in particle size [70]. Such parameters are not only determining the size of the produced nanoparticles, but they also determine their electrostatic potential which is a measure of dispersion stability. It may be possible to control particle size distribution and magnetisation properties through the manipulation of testing conditions such as stoichiometry, pH, Ionic

strength, temperature, etc [71].Therefore, the most efficient way of producing SPIONs that can readily be dispersed in water is often considered to be the application of iron salt co-precipitation into alkaline solutions.

The following phase in the production of SPIONs is to modify their surfaces after the iron oxide core has formed. Due to the low solubility and high agglomeration rates under physiological conditions, uncoated SPIONs present an issue that could result in precipitation and potentially blocking blood vessels [62]. The aim of this alteration is to increase the biocompatibility of SPIONs through a wide range of materials, e.g. carboxylic and amine groups, surfactants, polymers or inorganic substances [72]. Such materials are designed to prevent agglomeration of SPIONs either electrostatic repulsion or steric stabilization. The surface modification can be integrated into the in-situ synthesis process, or performed subsequently, depending on which method is needed to perform additional procedural steps.

In preparing SPIONs, the process of surface modification is a key step that significantly contributes to their improved performance in different applications. For SPION surface engineering, stability, biocompatibility, and blood half-life are the three main design factors [73]. By minimizing the particles' aggregation, which is necessary for their function inside biological systems, surface modifications improves the stability of the particles. Additionally, it provides biocompatibility, which minimises undesirable effects and enables particles to be guided more easily through the body. Lastly, this modification will extend SPIONs half-life in the bloodstream for a longer period and ensure that they have an increased time to circulate which is essential for their effectiveness as drug carriers or contrast agents.

The surface of SPIONs is frequently modified with a range of compounds, including polyethylene glycol, dextran, albumin, dendrimers, and oleic acid, among others [73]. However, β-CD needs special attention due to its distinctive advantages. A naturally occurring cyclic oligosaccharide called β-CD has several benefits for changing the surface of SPIONs. It can improve SPIONs' solubility and stability as well as promote their biocompatibility. Additionally, because of its structure, β-CD is a great

candidate for applications involving drug administration since it can encapsulate other molecules. This enables therapeutic agents to be administered directly into target sites, improving the efficacy of therapy and minimising potential side effects [74].

In terms of being environmentally friendly, green, β-CD coated SPIONs also have some advantages. Notably, the production of β-CD does not involve the use of toxic substances, which is a major advantage from an environmental perspective [75]. Furthermore, both β-CD and iron oxides are non-toxic and biocompatible, making them safe for use in various applications, including biomedical ones. However, it's important to note that while the materials themselves are green, the full environmental impact also depends on the synthesis process of the nanoparticles. In this respect, it should be noted that environmentally friendly solvents and conditions can also be applied in a green manner as regards the coating of SPIONs with β-CD . This will also diminish the environmental impact of the production processes for β-CD coated SPIONs.

Figure 2.9 provides a schematic illustration of a SPION coated with β-CD . Detailed information related to β-CD can be found in Section 2.4.2.

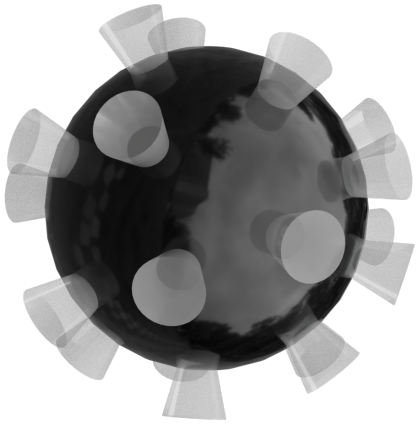

Figure 2.9. Schematic Illustration of β-Cyclodextrin Coated SPION.

2.4 Cyclodextrins (CDs)

The evolution of cyclodextrins dates back to the nineteenth century in France, where Antoine Villiers a pharmacist and chemist studied the effects of enzymes on different carbohydrates [76]. In the period from 1891 to 1911, extensive efforts were made to understand and characterise these substances after their discovery. The first person who made it possible to understand cyclodextrins was Schardinger [77]. He is known for not only outlining their fundamental properties but also for explicating their capacity to form complexes. Such pioneering work made Schardinger recognized as a "father" of cyclodextrin chemistry. Schardinger also found that starch sources, such as potatoes, rice and wheat, could be converted to cyclodextrins by various kinds of bacteria in the process of digestion resulting in an appreciable influence on their formation [76] [77].

The study of cyclodextrins' conformations, spectroscopic data, has been extensively investigated between 1950 and 1970 [78]. Cyclodextrins have been used for numerous industrial applications since 1970, primarily in the pharmaceutical and food sectors [77]. The first cyclodextrin-based chromatographic columns were commercialized in 1984, which was also the period when many cyclodextrin-based catalysts were being developed for biomimetic chemistry and other applications [78]. Today, cyclodextrins continue to play an important role in scientific research and development through their presence on more than 2000 academic publications per year. This demonstrates their increasing importance and applicability in a wide range of fields. It is clear that they will remain at the forefront of a number of scientific discoveries for many years to come as we uncover further aspects of cyclodextrin's flexible properties.

2.4.1 The Chemistry of Cyclodextrins: Structure, Properties, and Complexation

Cyclodextrins, an exceptional class of cyclic oligosaccharides, represent industrially synthesized macrocycles. As seen in Figure 2.10, they consist of glucopyranose

units interconnected by α-1,4 glycosidic linkages, forming uniquely-shaped, macrorings [79] [80]. This unique structure, together with their wide range of application possibilities, contributes to the importance of cyclodextrins in both academic and industrial applications.



Figure 2.10. Structure of cyclodextrins [80].

The cyclodextrins in this family can mainly be divided into three types: α-cyclodextrin, which has six glucopyranose units; β-cyclodextrin; and γ-cyclodextrin, which contain seven and eight units, respectively [78]. They are made from the enzymatic conversion of starch, a widely available and renewable source, thereby proving their eco friendly nature. A comprehensive comparison of the overall characteristics for alpha, beta and gamma cyclodextrins is presented in Figure 2.11.

Properties	α-CD	β-CD	γ-CD
Empirical formula	$C_{36}H_{60}O_{30}$	$C_{42}H_{70}O_{35}$	$C_{48}H_{80}O_{40}$
Molecular weight (g/mol)	972	1135	1297
Glucopyranose units	6	7	8
Cavity diameter (nm)	0.47–0.57	0.60–0.78	0.83–0.95
Internal cavity volume (nm^3)	1740	2620	4720
Number of water molecules in the cavity	6	11	17
Aqueous solubility (g/L)	129.5	18.4	249.2
Temperature of degradation (°C)	278	298	267

Figure 2.11. Properties of cyclodextrins [81].

Cyclodextrins are an intriguing aspect of biological architecture, as they have a very special structure. This structure is characterised by a lipidic central hole, which

contrasts to an hydrophilic surface on the outside. The unique orientation of their hydroxyl groups, where the primary hydroxyl group occupies a narrow margin between the cone and the secondary units are aligned parallel to the broader edge, is what gives them molecular characteristics [82].

The encapsulation potential of cyclodextrins is also evident in their impressive host-guest interaction profile.Their interesting trait confers a unique ability for cyclodextrins to function like molecular containers and is capable of containing several molecules at once. Cyclodextrins are able to interact with a wide range of molecules to form complex mixtures, equipped with a hydrophobic cavity that differs from its polar exterior. This includes alkyl glycosides, chiral compounds, branched or cyclic alkyl groups, aromatic molecules, and proteins [83]. Such complex forms allow cyclodextrins, which greatly contributes to their adaptability across a range of industrial sectors such as medicine, textiles, cosmetics and food, an important role in the production of stable host-guest complexes [82] [83].The ability of a guest molecule to fit inside the cyclodextrin cavity is crucial in determining the strength of the host-guest interaction. Considering the hydrophobic attributes of the cyclodextrin cavity, it tends to form more efficient bonds with organic molecules that exhibit hydrophobic interactions and less effectively with those that have hydrophilic or polar chemical functional groups. In Figure 2.12, a diagrammatic illustration of the host-guest interaction is provided.

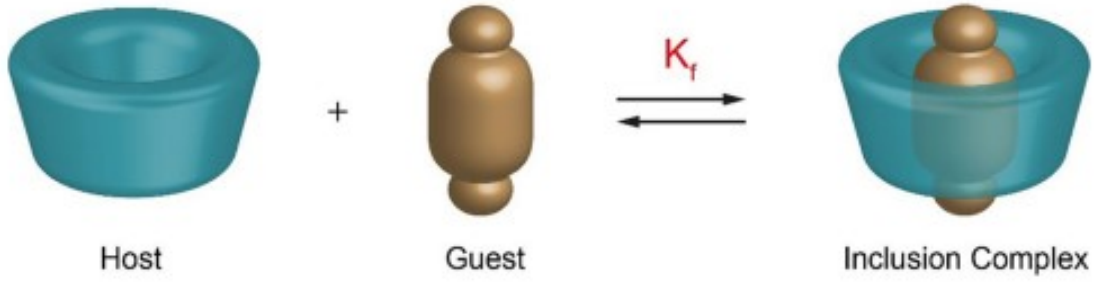

Figure 2.12. Schematic representation of an optimal host-guest interaction in cyclodextrin-based systems.

Cyclodextrins display a variety of structures representing the cyclodextrin to

guest ratio within their field of host-guest complexes. Although other types such as 1:2, 2:1, 2:2, 3:1, etc. are also reported, the most common complex form is 1:1 [84]. The diversity of cyclodextrin complexation, which is largely driven by enthalpy and disfavor entropy, influences binding kinetics and calculation of bound constants based on biophysical data [84].

Stability is another defining feature of cyclodextrins. The sugar polymers exhibit excellent durability in water and certain organic solvents, while being very stable under alkaline conditions. However, they are susceptible to hydrolysis, leading to ring opening and subsequent formation of different linear oligosaccharides and glucose units in acidic environments [83].

In conclusion, cyclodextrin displays an exceptional fusion of complex structural features and high functionality. They represent an environmentally friendly and promising tool in scientific advances because of their sustainable provenance from renewable resources, as well as their exceptional capacity to form complex mixtures with a diverse number of guest molecules. A promising path to breakthroughs in the field of transformation and sustainable scientific progress is provided by the enormous potential of cyclodextrins for innocative applications.

2.4.2 β-Cyclodextrins

β-cyclodextrin is one of the main members of the cyclodextrin family, a group of cyclic oligosaccharides with numerous applications in different sectors. Comprised of seven glucopyranose units, β-CD presents a unique molecular structure that is the basis for its impressive capabilities and versatile applications. β-CD is described by Roquette [85] as a chemical that normally appears as a white, or nearly-white, amorphous or crystalline powder.

Since its ease of production, low cost and internal cavity dimensions which are capable of accommodating a large number of guest molecules, β-CD has been regarded

as the best option for cyclodextrin [86]. Despite possessing the lowest solubility among its counterparts, a factor correlated with intramolecular hydrogen bonding, its appeal is enhanced due to its non-irritating, non-mutagenic nature and sustainability. The fact that its solubility in water can be greatly increased through chemical or enzymatic reactions makes β-CD %95 more usable among other cyclodextrin varieties [81]. Additionally, β-CD stands out as the most active cyclodextrin type in terms of hemolytic activity [81].

In the β-CD, C3 hydroxyl groups next to the C2 hydroxyl groups can create hydrogen bonds with each glucopyranose unit. This interaction gives the molecule a strong structure by forming a secondary hydrogen scaffold inside of it,as illustrated in Figure 2.13. As a result, these hydrogen bonds restrict β-CD's capacity to form bonds with other water molecules in the environment, decreasing its solubility. This property is thought to be the cause of β-CD's substantially lower solubility in water when compared to other cyclodextrin forms. Although it is also recognized as a benefit, β's poor solubility makes precipitation and separating throughout the manufacturing process simple [87].

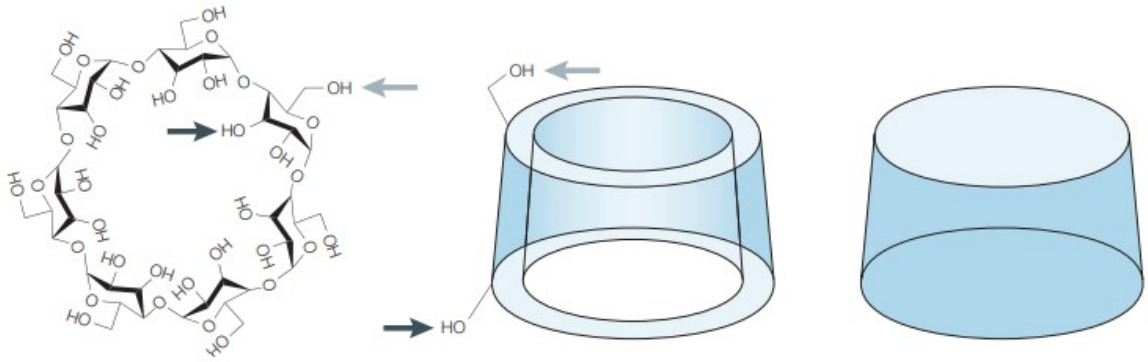

Figure 2.13. Chemical structure of β-Cyclodextrin [79].

Cyclodextrins have been introduced since the 1980s into different industries and, together with a finding of no apparent adverse effects if properly applied, they have stimulated their manufacture and diversified their applications [88]. Nearly 100 new cyclodextrin types, such as methylated and hydroxylated derivatives of β-CD', have been made accessible at affordable costs in addition to the hundreds of tons of alpha, beta and gamma cyclodextrins that are manufactured [87].

β-CD's play an essential role in the pharmaceutical industry as a solubilizing agent for drugs that are not sufficiently soluble in water and thus improve their controlled release. Therefore, this function increases the bioavailability of drugs and improves the quality of treatment. In addition, it can improve stability of certain unstable drugs which may increase their effectiveness in the application. In addition to the text description, the key features of cyclodextrins such as their potential as a drug carrier, their hydrophobic cavity, hydrophilic exterior, biocompatibility, protective capability, and enhanced solubility are visually represented in Figure 2.14 for a more intuitive understanding.

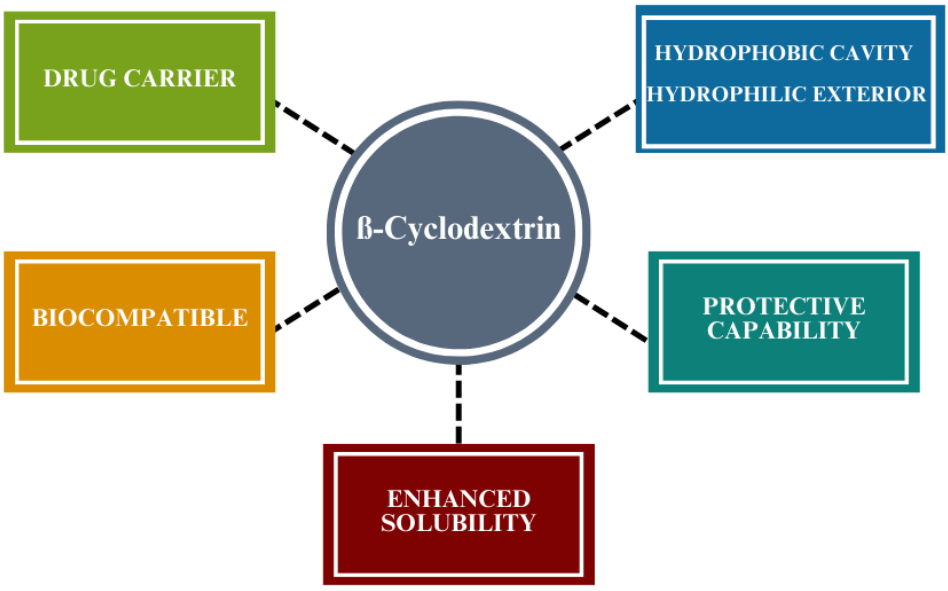

Figure 2.14. Schematic illustration of the key features of β-Cyclodextrin.

2.5 Design of SPION-Interacted Polymersomes

Interdisciplinary efforts to underpin progress in the area of drug delivery have become a driving force. This is clearly exemplified through the logical design and development of SPION-interacted polymersomes. Such systems, which can respond to a broad range of stimuli and thus offer huge promise in the area of targeted drug delivery, are an excellent example of multimodal systems.

In the specific system examined in this study, the polymersomes are formulated from Polyethylene Glycol (PEG) and 2-(Diethylamino)ethyl Methacrylate (DEAEMA). Moreover, the units of ferrocene are incorporated due to their distinctive redox-responsive properties. A four unit crosslinker, which is crucial to maintain the structural framework of the system, adds further strength to those polymersomes. A crosslinker that's added to the polymeric system is further enhancing the structural integrity of these polymers, which has been essential for their stability. Such an intricate design ensures a harmonious interaction between components, increasing the performance of the system.

A significant novelty in this design could potentially be seen in the strategic linkages between Ferrocene and β-CD, which were chosen for their capacity to interact with magnetic characteristics. The β-CD in this design does not merely act as an passive component but rather constitutes a vital instrument to mediate the complex interactions within the system, as seen in Figure 2.15. It enables a special interaction with the SPIONs, recognized for their magnetic properties, and ferrocene units, integrated due to their distinctive characteristics.This key interaction inside the system is further promoted by the ferrocene units' optimal accommodation in the inner cavity of the β-CD. Overall, it provides a clear indication of promising developments in the area, demonstrating the potential of such multimodal systems for controlled and targeted drug delivery applications.

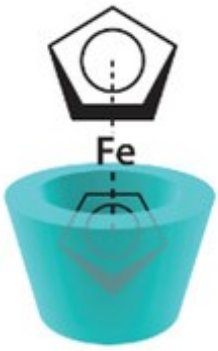

Figure 2.15. Schematic illustration of interaction between β-CD and Ferrocene units.

2.5.1 Polyethylene Glycol

Polyethylene Glycol, more commonly known as PEG, is a versatile polyether compound that is formed through the polymerization of ethylene oxide monomers [89]. PEG is distinguished, in particular by its hydrophilic and semi-crystalline nature. The fact that its physical characteristics, including its viscosity, are strongly influenced by its molecular weight is one of the most striking characteristics of PEG. As seen in Figure 2.16, the complexity of its chemical composition is revealed by a more detailed examination of its molecular structure [90].

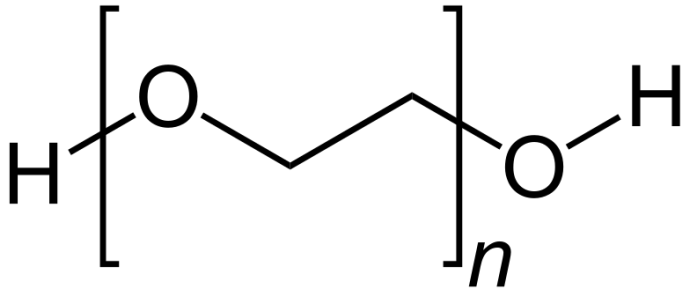

Figure 2.16. The repeating unit of the Polyethylene Glycol chain.

PEG significantly reduces the tendency of particles to aggregate and provides steric stabilisation, which enhances the stability of formulations during preservation and use as a nonionic hydrophilic polymer with stealth properties. Stealth properties, which reduce the immune system's recognition and lead to an increase in the circulatory

time of the drug carriers. This leads to an increased probability of the encapsulated medicinal product reaching its intended target, which contributes to improved therapeutic efficacy [91].

PEG is a polymer that has been extensively utilized in the biomedical field due to its distinct characteristics. It has been a material of choice for many types of medical applications, particularly as regards the delivery of drugs, because of its water solubility, biocompatibility, low toxicity and resistance to protein adsorption [91]. In the construction of polymersomes, PEG's hydrophilic properties are critical in forming the outer shell. This shell acts as a 'cloak,' protecting the encapsulated drugs from the immune system. Therefore, this shielding effect, often referred to as 'stealth,' allows for a prolonged period of circulation within the body. The enhanced circulation leads to a higher probability that the medicine will achieve its target, leading to an optimisation of therapy effectiveness [92]. In addition, PEGylation is essential to maintain the stability of these drug delivery systems. It decreases the aggregation tendency of particles, providing steric stabilization. This quality is paramount to ensuring the formulations' robustness during storage and use. Consequently, PEG does not only function as a material carrier but also significantly enhances the performance and safety of therapeutic agents embedded in polymersomes.

2.5.2 2-(Diethylamino)ethyl Methacrylate

The key polymer in biomedical applications, with special properties and extensive use for creating effective drug delivery systems, is 2-Diethylamino)ethyl Methacrylate (DEAEMA) as seen Figure 2.17. DEAEMA is particularly suited for the formulation of "smart polymersomes, due to its pH-responsive nature [93]. In particular, DEAEMA provides the resulting polymers with a special ability to react to changes in environment pH, enabling encapsulated therapeutic products to be released as carefully as possible and enhancing their efficacy and specificity. The ability to adapt to a variety of pH levels with its biocompatibility makes DEAEMA an important force in developing new drug delivery systems and other biomedical applications.

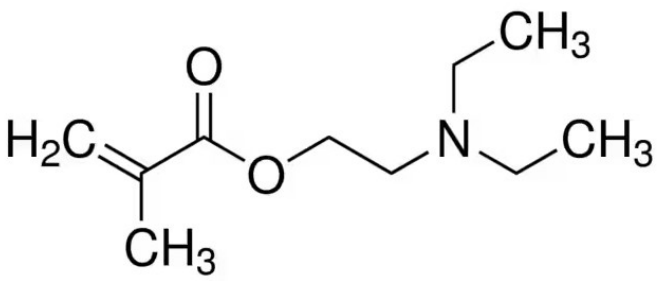

Figure 2.17. Chemical structure of DEAEMA.

In addition to its pH-responsive properties, DEAEMA's polymerizability is beneficial in creating robust and stable polymersomes. Its functional groups are highly modifiable, allowing researchers a great deal of flexibility for creating unique drug delivery systems. This quality, together with the capacity to combine with other substances to produce copolymers, increases the application potential of DEAEMA in a variety of purposes. The importance of DEAEMA in challenging the limits of biomedical engineering is shown by its versatility and flexibility.

2.5.3 Ferrocene

Ferrocene has been given considerable attention in various areas such as materials science, chemistry, biology and for its distinctive sandwichlike structure owing to its unique properties. As described in Figure 2.18, a combination of two cyclopentadienyl rings connecting to the central iron atom has shown that ferrocene and its derivatives can be beneficial for a diverse array of applications, ranging from catalysts to medical products. [94].

In addition to being a potential candidate for cancer therapy, ferrocene's special qualities, such as its capacity to produce reactive oxygen species, its redox activation, and its lipophilic characteristics, also give rise to opportunities for other biomedical uses, such as the modification of polymeric nanocarriers. [95] [96] These characteristics may be used to modulate drug release profiles in polymersomes, among other functions. In conclusion, ferrocene has opened a promising path in biological research due to its

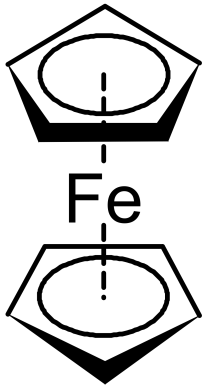

Figure 2.18. Chemical structure of Ferrocene.

distinct features.

In this work, 2-(methylacryloyloxy)ethyl ferrocencarboxylate (FcMA) has been added as a novel ferrocene unit to block copolymer system, as seen its chemical structure Figure 2.19. Through free radical polymerization methods, 2-methylacryloxyethyl ferrocencarboxylate, a monomer that contains ferrocene and has an active methacrylate group, can be simply polymerized.

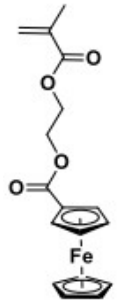

Figure 2.19. Chemical structure of FcMA [97].

S. Moreno et al. describe the synthesis of FcMA unit [97]. In their work, this unit was particularly pointed out for its contribution to the redox and pH-responsive properties of polymersomes. In the following sections of this thesis, additional studies on their inclusion in our block copolymer system are discussed.

2.5.4 Cross-Linkers

The crosslinkers are an essential part of polymer science which has a major role to play in defining the structure of the entire network as they act as bridging links among different polymeric chains, and thus greatly affecting their properties for final materials [98].

In the current study, two different cross-linkers were used to generate polymersomes. The ferrocene-free polymersomes were fabricated using 3,4-dimethyl maleic imidobutyl methacrylate (DMIBMA), while 3,4-dimethyl maleic imidohexyl methacrylate (DMIHMA) was used in the construction of the ferrocene-containing polymersomes.

3. METHODS

3.1 Materials

Iron(II) Chloride Tetrahydrate ($FeCl_2.4\,H2O$), Iron(III) Chloride Hexahydrate ($FeCl_3.6\,H2O$), Hydrochloric Acid (ACS reagent, 37%) (HCl), Ammonium Hydroxide (ACS Grade ≥28-30) (NH_4OH), Sodium Phosphate Dibasic Heptahydrate (ACS reagent, 98.0-102.0%) ($Na_2HPO_4.7\,H2O$), Sodium Phosphate Monobasic Monohydrate (ACS reagent, ≥98%) ($NaH_2PO_4.H2O$), β-Cyclodextrin (ACS reagent, ≥97%) ($\beta-$CD), Sodium Chloride (ACS reagent, ≥99%) (NaCl), Tetrahydrofuran (ACS reagent, ≥99%) (THF) were supplied by Sigma Aldrich. Dialysis membrane (MWCO 12-14 kDa) was bought from Spectrumlab.

The block copolymers used in this thesis were provided by the Leibniz Institute of Polymer Research Dresden. Table 3.1 provides detailed compositions of block copolymers (BCPs) used in the study for a complete comprehension [99] [97].

Table 3.1. Detailed Compositions of the Block Copolymers

Sample	PEG	DEAEMA	FcMA	Cross-Linker	Mw (kg/mol)
BCP1	45	88	-	DMIBMA-23	24.5
BCP2	45	56	20	DMIHMA-24	26.6

3.2 Methods

3.2.1 Synthesis of β-CD Coated Superparamagnetic Iron Oxide Nanoparticles

β-CD coated iron oxide particles were synthesized using a modified version of a previously reported procedure [75]. The synthesis of magnetic nanoparticles has been performed at room temperature by a co-precipitation method. Initially, 12.0 ml of an acidic solution of ($FeCl_2$.4 H2O) (15.9 g in 20 ml of 2M HCl) and 48.0 ml of an acidic solution of ($FeCl_3$.6 H2O) (13.52 g in 50 ml of 2M HCl) were mechanically stirred together. The stirring was continued during the slow addition of 600 ml of an aqueous 0.7M (NH_4OH) solution into the beaker. As shown in Figure 3.1, this process continued until the color of the mixture changed from yellow to black, indicating the successful formation of magnetite.

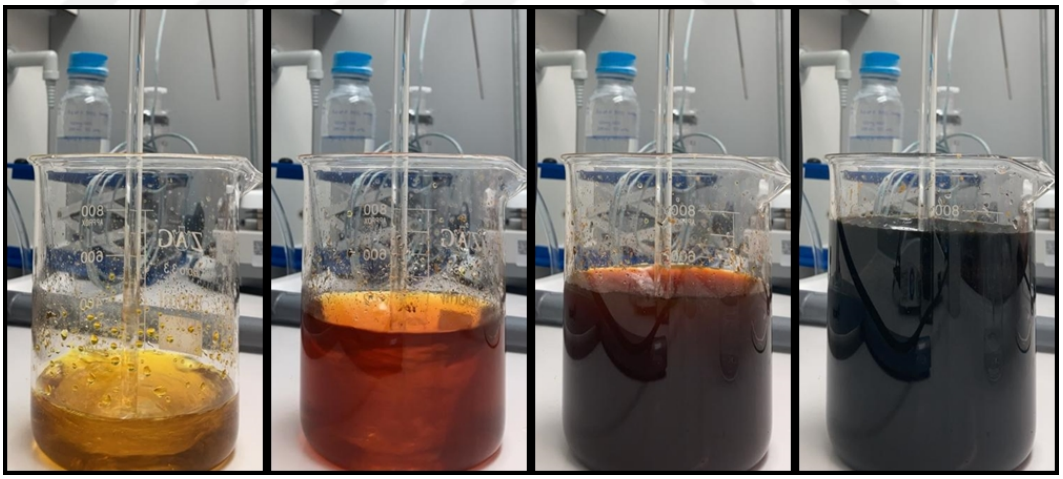

Figure 3.1. The formation of SPIONs following the addition of NH_4OH.

Subsequently, the particles were magnetically decanted from the solution with the help of a neodymium magnet and washed several times with 800 mL of pure water until the pH of the wash liquid remained neutral. The washed magnetite particles were then dried in an oven at 70°C for 24 hours. Figure 3.2 shows dried bare SPIONs.

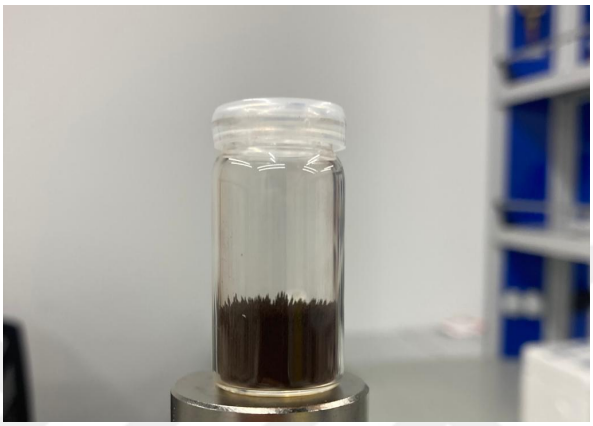

Figure 3.2. Dried ferrophase sample after the 24-hour drying process.

For the coating step, the obtained ferrophase (4.32g) was vigorously mixed with 0.4g of β-cyclodextrin ($C_{42}H_{70}O_{35}$) and 24 mL of deionized water, and the mixture was maintained at a acidic pH, as seen Figure 3.3.

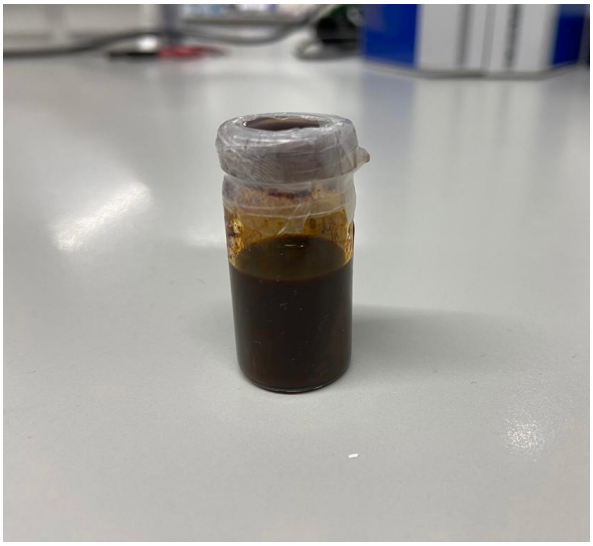

Figure 3.3. β-CD coated SPIONs.

3.2.2 Characterization of β-CD Coated Suparparamagnetic Iron Oxide Nanoparticles

The synthesized β-CD coated SPIONs were used to a wide variety of characterization processes. The solid content, size distribution and structural properties of the nanoparticles have been determined during this process. Furthermore, magnetic properties have been assessed using a Vibrating Sampling Magnetometer. Then using the Fourier Transform Infrared Spectroscopy (FTIR) and Thermogravimetric Analysis (TGA), were explored the structure's chemistry and thermal properties. At the same time, experiments were carried out to assess the stability of nanoparticles under varying pH conditions. All these analyzes helped to create a comprehensive profile of the β-CD coated superparamagnetic iron oxide nanoparticles.

3.2.2.1 Solid Content Analysis

In solid content analysis firstly, the weight of an empty watch glass has been determined and recorded with a precision balance. Following that, 100 µL of the β-CD coated SPION sample was poured over the watch glass and dried overnight in a high temperature drying oven. The total mass of the dry sample and the watch glass was again measured with a precision balance at the end of the drying process. The solid content of the dry sample was determined by taking into account the difference between the final weight and the initial weight of the watch glass.

3.2.2.2 Size and Polydispersity Index Measurement

The samples' size and polydispersity index (PdI) were measured using the Dynamic Light Scattering (DLS) method. The Zetasizer Nano S90 (Malvern Instruments, UK) was used for this measurement. Distilled water was used to dilute each sample before examination in order to prevent the possibility of nanoparticles clumping together and generating inaccurate size measurements.

3.2.2.3 Morphological Characterization

Transmission electron microscopy (TEM) was used to analyze the morphology of the synthesized β-CD coated SPIONs. Samples were first diluted and then dropped onto the 300 mesh carbon-coated copper grids and left to dry for couple of hours in order to analyze TEM. This step is crucial for nanometer structures to be viewed and learned about their dimensions.

A Libra 200 transmission electron microscope was used to perform a morphological study on synthesized β-CD coated SPIONs. The microscope is equipped with a field emission gun and a monochromator to ensure the highest resolution imaging and detailed analysis of energy levels. The high contrast that can lead to more detailed images is mainly enhanced by the Omega-type energy filter and HAADF detector mounted on the microscope. In this method, the morphological properties of the β-CD coated SPIONs were carefully examined while the diameters of the nanoparticles were quantified using software such as Image-J [100].

3.2.2.4 Vibrating-Sample Magnetometer

The LDJ Electronics Model 9600 Vibrating Sample Magnetometer (VSM) was used to analyze the magnetic characteristics of β-CD coated SPIONs and bare SPIONs. These analyses have made it possible to accurately quantify the properties of particles based on magnetisation. At the conclusion of the analysis, the magnetic characteristics of both bare SPIONs and SPIONs β-CD were compared. Lastly, determining the potential uses of these nanoparticles mainly depends on the magnetic properties of the β-CD coated SPIONs.

3.2.2.5 Fourier-Transform Infrared Spectroscopy

The Vertex80v FT-IR Spectrometer (Bruker) was used to conduct the FT-IR spectroscopy analysis. This analysis was used to characterize β-CD, SPIONs, and β-CD coated SPIONs. The Golden Gate Diamond ATR unit and the MCT-Detector were utilized for the measurement, which was carried out in the wavelength range of 4000-600 cm^{-1} with a resolution of 4 cm^{-1} and 100 scans for each measurement. The obtained spectra were used to determine the presence of bonds and chemical structures. These detailed analyses enhanced our understanding of the β-CD coated SPIONs' chemical structures and potential chemical interactions.

3.2.2.6 Thermogravimetric Analysis

The thermal properties and stability of the synthesized β-CD coated SPIONs were assessed using thermogravimetric analysis (TGA). This analysis was conducted using the TGA Q 5000 model instrument (TA Instruments), a device that evaluates weight losses at various temperatures. The TGA provides extensive information about thermally induced physical and chemical changes, as well as the thermal stability of materials.

3.2.2.7 Investigation of SPIONs' pH Sensitivity

The behavior of β-CD coated SPIONs under different pH conditions was analyzed. Specifically, their size and PdI were measured at various pH values using the Zetasizer Nano S90 (Malvern Instruments, UK) DLS system. These measurements provided important information about the stability of the β-CD coated SPIONs under different pH conditions.

3.2.2.8 Time-Dependent Stability Assessment of β-CD coated SPION

Testing the stability of synthesized β-CD coated SPIONs is critical for potential applications of these nanoparticles. A Zetasizer Nano S90 (Malvern Instruments, U.K.) model DLS instrument was used to measure size at certain times during stability testing. The changes in the physical properties of nanoparticles over time are determined by these measurements and enable monitoring of their sustained stability for a period of time.

3.2.3 Preparation of Polymersomes

In this section, two distinct polymersome formulations are discussed. Firstly, polymersomes without ferrocene were produced as a control group. Then, ferrocene-containing polymersomes are generated; they have been precisely designed to interact with the β-CD coated SPIONs. Importantly, same experimental conditions are followed and the same experiments are conducted on both polymersome types to enable a valid comparison of their respective properties and behaviors.

3.2.3.1 Preparation of Ferrocene-Free Polymersomes

The method developed by Gaitzsch et al. was adapted to synthesize Ferrocene-free Crosslinked Polymersomes using the following simplified procedure [99]: 10 mg block co-polymer (BCP-1) dissolved in 10 mL of 0.01 M HCl (pH 2) and stirred for some hours until the entire BCP-1 was totally dissolved. The solution was passed through a nylon syringe filter (0.2 µm) to eliminate any residual particulates. Next, 0.01M NaOH was gradually added to the filtered BCP-1 solution until a pH of 8 was reached to achieve self-assembly. After stirring for 3 days, the final solution was passed through a cellulose ester syringe filter (0.8 µm) and placed in the UV chamber under irradiation for 60 seconds.

3.2.3.2 Preparation of Ferrocene-Containing Polymersome

Building on the methodology developed by Moreno et al., the following procedure was followed to fabricate ferrocene polymersomes [97]. Initially, 10 mg of block copolymer (BCP-2) was dissolved in 2 mL of tetrahydrofuran (THF). A turbid solution was formed by adding 4 mL of water gradually after that. This solution was stirred consistently for a period of 72 hours. Afterwards, the THF was slowly evaporated at room temperature, and 6 mL of 10 mM NaCl solution at pH 8 was incorporated. This solution was stirred overnight and subsequently filtered through a 0.45 µm syringe filter for DLS measurement. Subsequently, the sample was exposed to 90 seconds of irradiation in a UV chamber prior to a second DLS measurement. As a final step, the solution was transferred to a dialysis membrane (MWCO 12-14 kDa) for an overnight dialysis against water, in preparation for the ultimate round of DLS measurements.

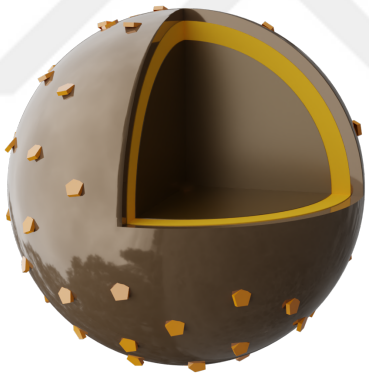

Figure 3.4. Ferrocene-Containing Polymersome.

3.2.4 Characterization of Polymersomes

A number of techniques were used to characterise the prepared polymersomes. The size, polydispersity index, and morphological characteristics are the primary aspects assessed.

3.2.4.1 Size and Polydispersity Index Measurement

The size and PdI of the polymersomes were measured using a Zetasizer Nano S90 (Malvern Instruments, U.K.) model Dynamic Light Scattering (DLS) equipment.

3.2.4.2 Morphological Characterization

Scanning Transmission Electron Microscopy (STEM) was used to carry out morphological characterization. In this process, a drop of polymersome was placed on the copper grid and dried. Significant knowledge about the physical characteristics and structures of polymersomes has been obtained from observations carried out by STEM.

3.2.5 Interaction Between SPIONs and Polymersomes

To investigate the surface interactions of polymersomes with SPIONs, a specific approach was used to both ferrocene-containing and ferrocene-free polymersomes. The following are the precise ratios applied in the procedure: Starting with a 1 mg/mL stock solution of SPIONs in distilled water, it was diluted to 0.1 mg/mL using a 0.5 mM PBS buffer. Further dilution with distilled water achieved a final concentration of 0.05 mg/mL, with the resulting pH measured to be approximately 7.4. This SPION solution was then mixed with a 0.5 mg/mL Empty-Polymersomes suspension in a 1:1 volume ratio, yielding final concentrations of 0.25 mg/mL for Polymersomes and 0.025 mg/mL for SPIONs. Following this, the mixture was allowed to incubate in the dark at room temperature with a speed of 50 rpm for 15 hours, after which the particle size was evaluated using DLS. Additional DLS measurements were taken both from the sample's supernatant and the pellet after the mixture was centrifuged at 4000 rpm for 15 minutes.

3.2.6 Characterization Study on SPION-Polymersome Interactions

Two different methods have been used in this section to characterise SPION Polymersome Interactions, namely the size and PdI measurements as well as morphological characterization

3.2.6.1 Size and Polydispersity Index Measurement

Zetasizer Nano S90 (Malvern Instruments, U.K.) was used to assess the size and PdI of SPION-Polymersome interactions. Important details regarding the size and distribution of nanocarriers are obtained by these measurements.

3.2.6.2 Morphological Characterization

Polymersome samples, which have interacted with SPIONs on their surface, were analyzed using STEM for morphological characterization. The samples were dried in a 300-mesh carbon-coated copper grids, which was then examined under the microscope. This method has been used in order to analyze how SPIONs are distributed within a polymersome and the morphology of interactions.

4. RESULTS and DISCUSSION

4.1 Characterization Results of β-CD Coated Superparamagnetic Iron Oxide Nanoparticles

4.1.1 Solid Content Analysis

In order to determine the quantity of the solid component within the β-CD coated SPION samples, a solid content analysis has been carried out. In the first place, an empty watch glass was weighed with a precision balance. Subsequently, a 100 µL sample of the β-CD coated SPIONs was placed onto the watch glass and dried overnight in a high-temperature drying oven. After drying procedure, a precision balance was applied to calculate the overall weight of the watch glass and the dried sample. Subtracting the initial weight of the watch glass from the final weight is then used to calculate the solid content of the dried sample. Through this method, it was determined that the solid content of the β-CD coated SPION sample was 110 mg/mL.

4.1.2 Size and Polydispersity Index Measurement

DLS was used to analyze the properties of β-CD coated SPIONs, specifically to determine their hydrodynamic diameter and Polydispersion Index (PdI). The analysis of a β-CD coated SPION sample has been carried out using two different methods. In the first scenario, the sample was diluted to 1mg/mL and subjected to direct measurement of DLS.

In the second scenario, the sample was centrifuged at 14.500 rpm for 20 minutes to isolate any potential aggregates from the nanoparticles. The supernatant was carefully removed and analyzed separately using DLS, while the pellet was re-dispersed with pure water and its characteristics were analyzed. Table 4.1 shows the corresponding

changes to the Z-average hydrodynamic diameter and PDI values. The data show that the specimens are uniform, and no significant signs of degradation have been observed.

Table 4.1. Hydrodynamic Size and PDI of Synthesized β-CD coated SPIONs

Sample	Size (nm)	PDI
β-CD coated SPIONs (1mg/mL)	51.8 ± 0.84	0.23 ± 0.009
β-CD coated SPIONs (Re-dispersed pellet)	56.9 ± 1.32	0.26 ± 0.003
β-CD coated SPIONs (Supernatant)	23.6 ± 0.51	0.22 ± 0.002

The hydrodynamic diameter of the β-CD coated SPION was 51.8 ± 0.84 nm, with a PdI=0.23 ± 0.009, which showed that monodisperse nanoparticles were produced. After centrifugation, the re-dispersed pellet showed a slight increase in size to 56.9 ± 1.32 nm and PDI to 0.26 ± 0.003, which may suggest an alteration in the size distribution during the separation process. Interestingly, the supernatant sample showed a considerably smaller size of 23.6 ± 0.51 nm with a PdI of 0.22 ± 0.002, indicating the presence of smaller particles or aggregates that remained suspended during centrifugation.

There is a need to note that the DLS provides information on the hydrodynamic diameter, which includes the particle core and any associated hydration layer or surface-associated molecules, thus, actual core sizes could be smaller. More reliable results were obtained through the analysis of TEM in the subsequent phase of the study.

4.1.3 Morphological Characterization

To gain a deeper understanding of the size distribution and morphology of synthesized β-CD coated SPIONs, TEM analysis was carried out in the next step. The β-CD coated SPION shown in Figure 4.1 displays a highly dispersed morphology with particles of mainly round and spherical shape at 1 mg/mL concentration. Using the ImageJ software, which provides an open platform for scientific image analysis, the average particle size was calculated to be 16±5 nm. This is confirmed by the DLS measurements, which tend to have greater hydrodynamic diameter when there are

hydration layers near the particles.

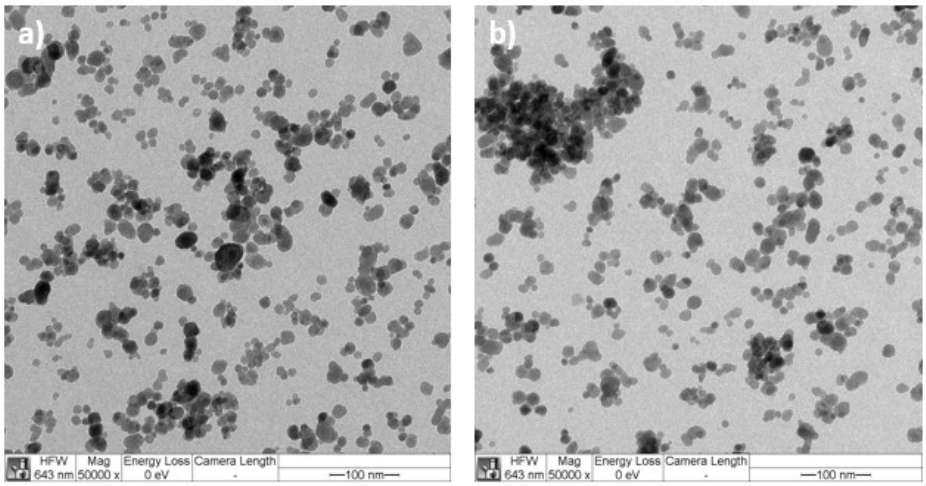

Figure 4.1. TEM Images of β-CD Coated SPIONs at 1mg/mL concentration, presented at 100 nm scale.

The supernatant phase obtained after centrifugation has been investigated to determine any potential changes due to the centrifugation process. The supernatant phase showed slightly more monodispersed distribution in comparison to the initial 1 mg/mL solution, as shown in Figure 4.2. The average particle size was found to be 12±3 nm, and the particles were still mainly spherical. Notably, the size difference between the original 1mg/mL solution and the supernatant fraction was not significant, indicating the robustness of the synthesis method.

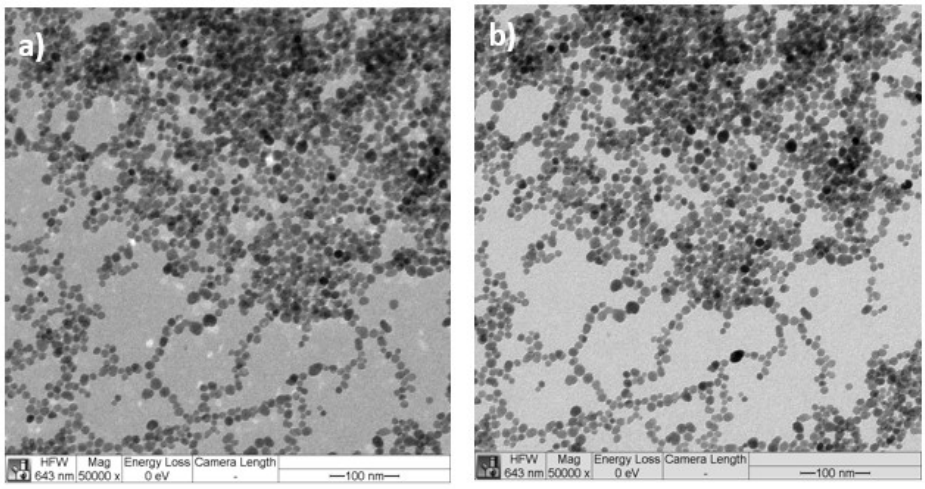

Figure 4.2. TEM Images of the supernatant phase of β-CD Coated SPIONs, at 100 nm Scale.

4.1.4 Vibrating-Sample Magnetometer

The Vibrating Sample Magnetometry (VSM) analysis carried out at room temperature, provided a crucial understanding of the influence of β-CD coating on the magnetic properties of SPIONs. The resulting magnetisation curve, as shown below in Figure 4.3, provides an excellent indication of the comparison.

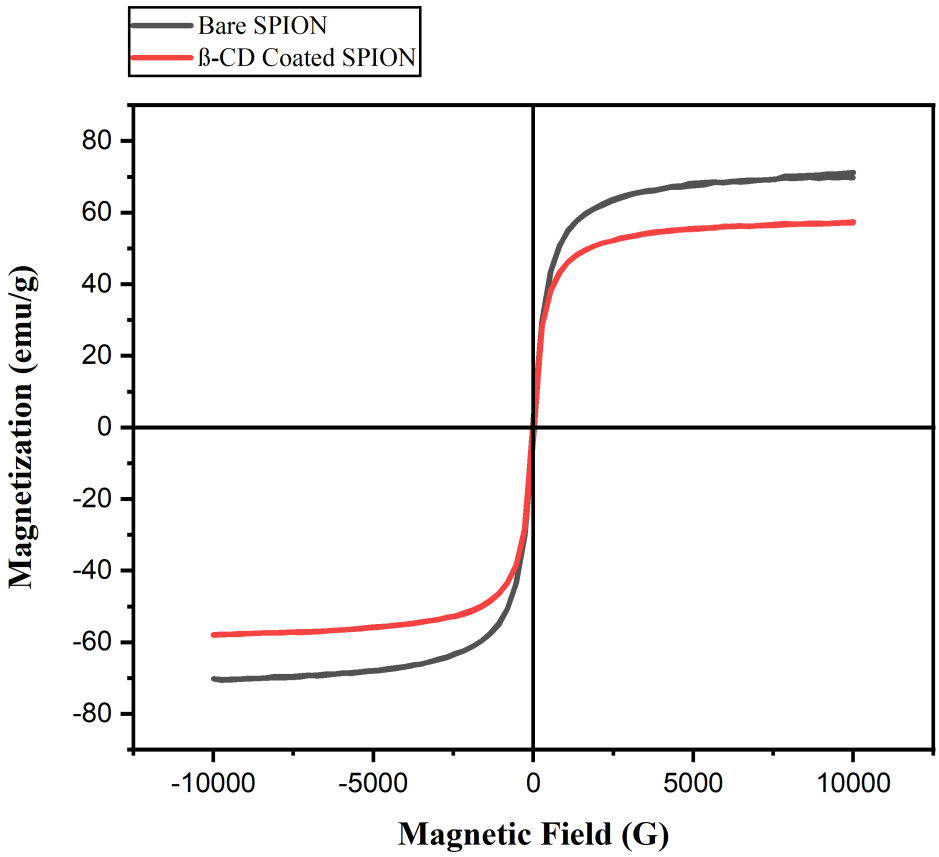

Figure 4.3. VSM analysis of Bare SPIONs and β-CD coated SPIONs.

The bare SPIONs showed a magnetization of 69.8 emu/g, whereas the β-CD coated SPION exhibited a reduction to 57 emu/g. This decrease in magnetization is attributable to the inherent physical and chemical attributes of the β-CD coating, which forms a protective barrier around the SPIONs, potentially altering the magnetic interactions. Thus, the impact of the coating on the magnetic properties of the SPIONs is clearly validated through these findings.

4.1.5 Fourier-Transform Infrared Spectroscopy

The analysis of the FTIR is intended to determine whether β-CD exists on the surface of SPIONs, or not. The corresponding absorption peaks for the SPIONs, β-CD and β-CD coated SPIONs are described in Figure 4.4. The peaks characteristic of both SPIONs and β-CD in the β-CD coated SPIONs spectrum provide additional evidence of the successful conjugation process.

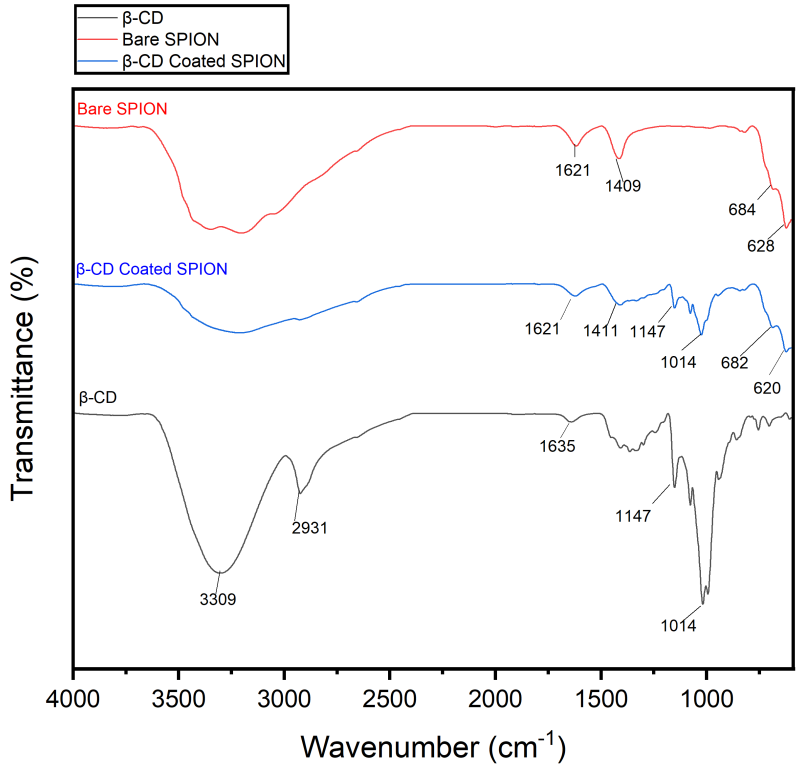

Figure 4.4. FTIR spectra of Bare SPIONs, β-CD, and β-CD coated SPIONs.

The characteristic peak for SPIONs, typically observed at 585 cm^{-1} (corresponding to the Fe-O vibrational peak), is present in the measured data, although slightly shifted to 628 cm^{-1} and 684 cm^{-1}. This shift may be caused by changes in sample preparation, particle size and possible interactions with the environment. Furthermore, a distinct peak at 1409 cm^{-1} was observed, aligning with the asymmetric stretching vibration of the Fe-O bond within the SPION structure.

Upon analyzing the spectrum of the β-CD coated SPIONs, peaks were identified,

assignable to both SPIONs and β-CD. Notably, the peak at 682 cm^{-1} and 620 cm^{-1}, corresponding to the Fe-O vibrational peak, substantiates the presence of SPIONs. Furthermore, the peak at 1621 cm^{-1} primarily originates from SPION, while the peaks at 1147 cm^{-1} and 1014 cm^{-1} correspond to the C-O-C stretching vibrations of β-CD. This observation underscores the coexistence of these components within the spectrum.

Lastly, a prominent peak at 3309 cm^{-1} signifies the free stretching vibration of the O-H bond of β-CD .Concurrently, a distinct vibration of the C-H bond at 2931 cm^{-1} was revealed through analysis, further emphasizing the complex nature of the sample.

In conclusion, the comprehensive spectral scrutiny furnishes compelling substantiation of the successful coating of β-CD onto the SPIONs. The presence of distinct peaks characteristic of both SPIONs and β-CD in the spectrum of the coated SPIONs substantiates the triumphant execution of this coating process. These findings underscore the successful realization of our objective in this pioneering research undertaking.

4.1.6 Thermogravimetric Analysis

To understand the thermal characteristics and heat resistance of chemical bonds on β-CD coated nanoparticles' surface, samples have been investigated in a specific temperature range during this analysis. Measuring the loss of weight at various temperature levels allow us to understand β-CD relative stability in terms of exposure to heat, as well as its duration on the nanoparticle surface.

Figure 4.5 illustrates the TGA results of bare SPIONs and β-CD coated SPIONs. The figure shows a gradual weight loss, attributing it to the thermal degradation of the β-CD coating as the temperature rises, while the iron core is unaffected.

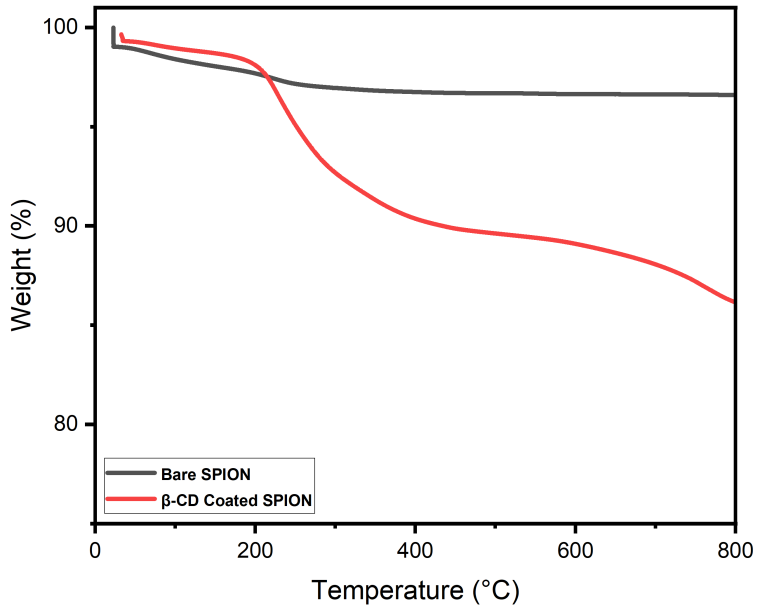

Figure 4.5. TGA Analysis of Bare SPIONs and β-CD Coated SPIONs.

In order to determine the thermal stability and durability of the β-CD coated SPIONs, thermogravimetric analysis plays an important role. These details give the criteria required to identify potential applications of nanoparticles within a wider temperature range. Moreover, important details about how nanoparticles will behave under a variety of temperatures are also provided in this analysis. Given that information, it will be possible to gain an overall understanding of the properties and performance of β-CD coated SPIONs.

4.1.7 Investigation of SPIONs' pH Sensitivity

Important aspects of our analysis are the pH sensitivity of β-CD coated SPIONs and potential effects on their stability in different conditions. It is vital to understand the characteristics of these particles under various pH conditions, so that their use in pH sensitive polymersomes can be optimised. Figure 4.6 shows a graph of the pH variations in the SPIONs samples that were analyzed. The SPIONs' particle size change when the pH level increase, as seen in this graph.

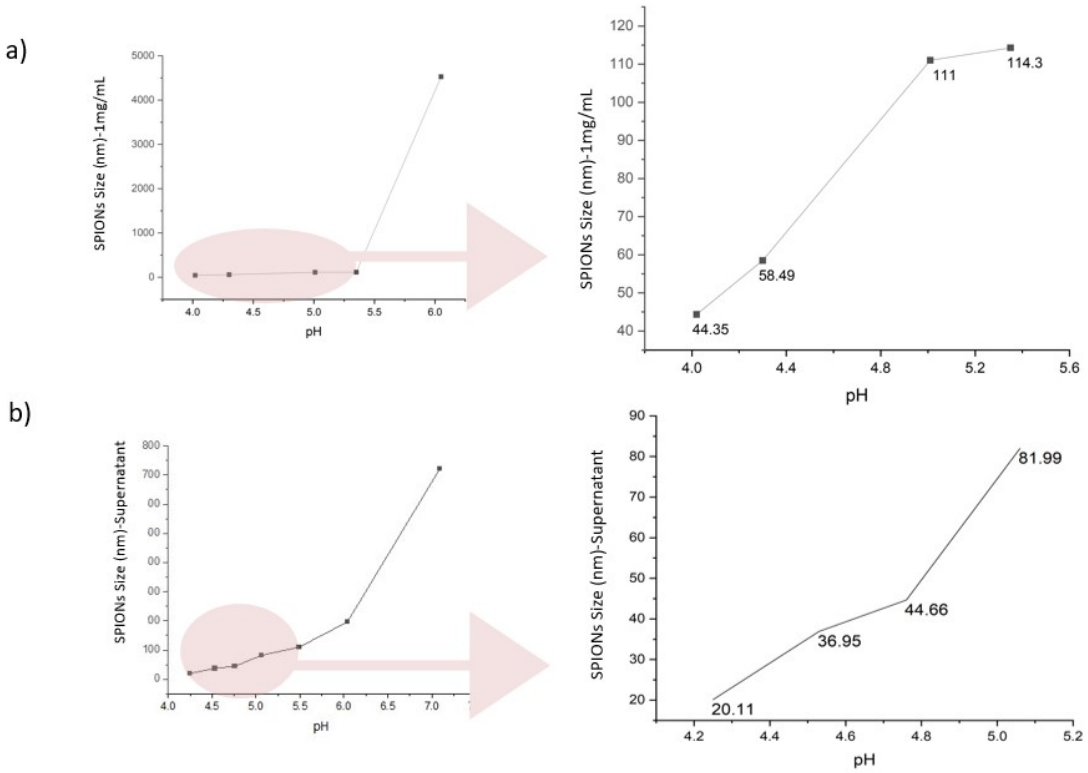

Figure 4.6. pH Alteration Study of β-CD Coated SPIONs Samples: (a) Sample with 1 mg/mL concentration; (b) Supernatant sample.

The original stock solution of directly produced, β-CD coated SPIONs exhibited a pH around 2.4. This solution was then diluted with distilled water to a concentration of 1 mg/mL, resulting in a pH reading of approximately 4. Subsequently, after centrifuging a 1 mg/mL sample for 20 minutes at 14,500 rpm, the pH of the obtained supernatant was determined, and a value of around 4.2 was obtained. Following these preliminary measurements, a pH alteration study was carried out on both the supernatant and the 1 mg/mL sample, as shown in Figure 4.6. It was observed that as the pH was adjusted towards 5, both samples exhibited signs of aggregation, increases in particle size, and most notably, visible precipitation.

A photograph of the precipitate sample due to the pH change is shown in Figure 4.7, following Figure 4.6. The visible precipitation points to the real impact of pH changes on SPION stability.

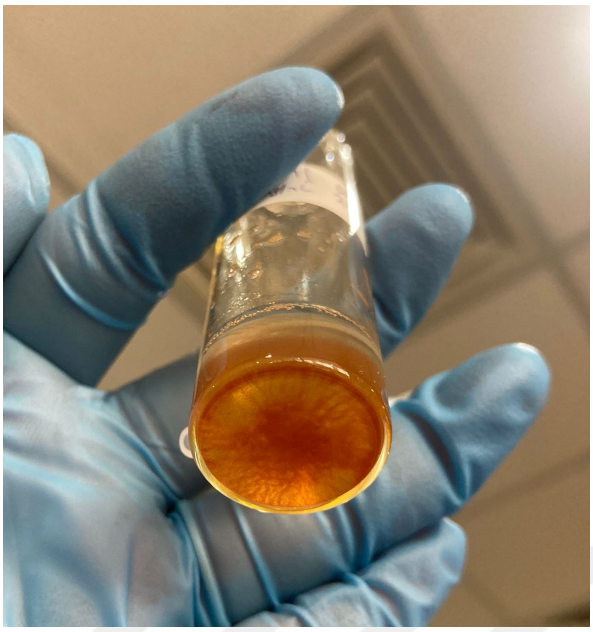

Figure 4.7. Visual Representation of Aggregation in β-CD coated SPIONs at pH 6.05.

4.1.8 Phosphate Buffered Saline (PBS)-Based pH Optimization

As can be seen from the previous sections, at pH 5 there is a very significant deterioration in β-CD coated SPION stability with visible precipitation.Considering the importance of maintaining a biological pH for usage, as well as the significance of employing these β-CD coated SPIONs in a pH-sensitive polymersome, it is essential to carry out an optimization research study. Therefore, the aim of this study is to ensure that β-CD coated SPIONs are stable in a PBS environment where pH stays at 7.4 and closer to physiological pH.

During the preparation process, the β-CD coated SPIONs, synthesized from the stock solution, were initially diluted to 1 mg/mL using pure water, resulting in a pH of approximately 4.2. The solution was then further diluted with a 0.5mM PBS buffer that had already been pre-adjusted to a pH of 7.4 to a concentration of 0.1 mg/mL. Remarkably, the SPIONs demonstrated stability at this biologically relevant pH (7.38). To verify the procedure, DLS measurements were performed at three distinct time intervals. As illustrated in Table 4.2, the results demonstrate consistent size and PdI values, highlighting the stability of this optimization process. Regarding working with

pH-sensitive polymersomes, this approach is very useful since it offers vital insights for sustaining stability and effectiveness in unique biological systems.

Table 4.2. Hydrodynamic Size and PDI of the β-CD coated SPIONs in PBS

Sample	Size (nm)	PDI
β-CD coated SPIONs (0.1mg/mL in 0.5mM PBS, pH 7.4)	53.65±0.24	0.20±0.01
β-CD coated SPIONs (0.1mg/mL in 0.5mM PBS, pH 7.4)	54.59±0.33	0.21±0.01
β-CD coated SPIONs (0.1mg/mL in 0.5mM PBS, pH 7.4)	39.35±0.39	0.15±0.01

4.1.9 Time-Dependent Stability Assessment of β-CD coated SPIONs

Monitoring of the longterm stability of β-CD coated SPION, a key factor for possible medical applications, will be carried out as part of this research. Since the initial measurement, these SPIONs have been carefully monitored. By using DLS, their stability is measured. Table 4.3 provides data collected from these measurement of the DLS. Incredibly, the β-CD coated SPIONs maintained their stability for seven months during which it was evident that they were both robust and reliable. It's noteworthy that these measurements pertain to various samples continuously diluted from stock solutions and measured at a concentration of 1 mg/mL. It is also important to note that, as the pursuit of ensuring their long term stability continues, these measurments are ongoing.

Table 4.3. Time-Dependent Stability of Hydrodynamic Size and PdI for β-CD Coated SPIONs

Sample	Size (nm)	PDI	Day
β-CD coated SPIONs	45.42±0.26	0.23±0.02	0
β-CD coated SPIONs	44.33±0.01	0.22±0.01	7
β-CD coated SPIONs	57.91±9.59	0.26±0.08	57
β-CD coated SPIONs	42.09±0.51	0.22±0.02	110
β-CD coated SPIONs	52.35±0.06	0.22±0.01	205
β-CD coated SPIONs	44.05±0.20	0.23±0.04	228

The statement suggests that there may have been slight variations over time in the size and PdI measurements of β-CD coated SPIONs. These variations may have

been caused by slight changes in the environment conditions, or minor inconsistencies over measurement procedures. Nevertheless, despite these minor variations, β-CD coated SPIONs are considered to be fairly stable. The implication is that even with some minor variations, the properties of the SPIONs remain suitable for their intended applications, and they are expected to perform reliably over an extended period.

4.2 Characterization Results of Polymersomes

This section discusses the results of characterisations for empty polymersomes formed from BCP1 and BCP2. For this purpose, measurements with DLS have been performed to gain a perspective on the size distribution and uniformity of the polymersomes. Additionally, TEM analyis was carried out to assess their morphological characteristics, which in turn, facilitated the visualization of these structures on a nanometer scale.

4.2.1 Size and Polydispersity Index Measurement

The Ferrocene-Free Polymersomes produced from BCP1 and the Ferrocene-Containing Polymersomes produced from BCP2 are the two different types of empty polymersomes that are subject of this section's size and PdI measurements.

4.2.1.1 Preparation of Ferrocene-Free Polymersomes

As discussed in section 3.2.3.1, Ferrocene-Free Polymersomes were produced from BCP1 at a concentration of 1mg/mL. In order to provide a comprehensive overview of their size distribution and polydispersity, DLS measurements have been carried out at three key stages of the polymersome preparation process. The three stages are "Before Crosslinking" ,"Before Crosslinking+Filtration" and "60s Crosslinking" Figure 4.8 gives a visual representation of the associated data. This sequence of measure-

ments has allowed for an in-depth understanding of how the size and uniformity of the polymersomes evolve throughout the preparation process.As a result, size data of the polymersome under basic conditions showed a size of about 64.4 nm.

		Z-Average	PdI
BCP1	Before Crosslinking	66.4 nm	0.17
	Before Crosslinking + Filtration	63.43 nm	0.16
	60 s Crosslinking	64.4 nm	0.15

Figure 4.8. DLS Measurements of Ferrocene-Free Polymersomes Produced from BCP1.

Additionally, pH cycle test was carried out between pH 4 and pH 8 to demonstrate the polymersome's ability to change size, as shown at Figure 4.9. The results obtained showed that the average size of the polymersomes was approximately 92 nm under acidic conditions and approximately 60 nm under basic conditions. These outcomes validate the polymersomes' pH-responsive behavior, thus providing solid evidence of the efficient pH switch mechanism inherent in the produced polymersomes.

4.2.1.2 Preparation of Ferrocene-Containing Polymersome

As discussed in section 3.2.3.2, Ferrocene Containing Polymersomes were produced from BCP2 at a concentration of 1mg/mL. The DLS measurement was performed at three critical points , "Before Crosslinking", "After 90 Seconds of Crosslinking," and "After 24 Hours of Dialysis", of the polymersome production process in order to gain an understanding of their size variations and distribution. Figure 4.10 provides a visual representation of the relevant data. A detailed understanding of how polymersome size and PdI change throughout the preparation process has been enabled by this sequential measurement. As a result, the diameter of polymersomes has been determined to be around 310 nanometres in accordance with basic conditions.

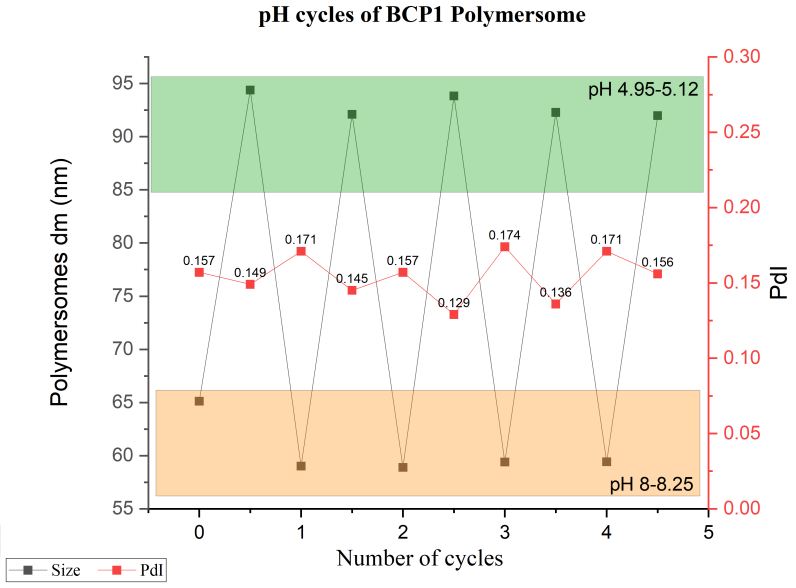

Figure 4.9. pH Cycle Study of FFP Produced from BCP1.

		Z-Average	PdI
BCP2	Before Crosslinking	487.3 nm	0.25
	After **90** s Crosslinking	346 nm	0.24
	After 24h Dialysis	310.2 nm	0.21

Figure 4.10. DLS Measurements of FCP Produced from BCP2.

To observe the polymersomes' reaction to changing pH levels, a pH cycle test has been performed in both acidic and basic conditions. The results, which can be seen in Figure 4.11, show a particular behavior whereby the size of polymersomes is altered by the pH environment. This trend is helping to support the pHresponsive nature of these structures, showing that they may be flexible and responsive under a variety of environmental conditions.

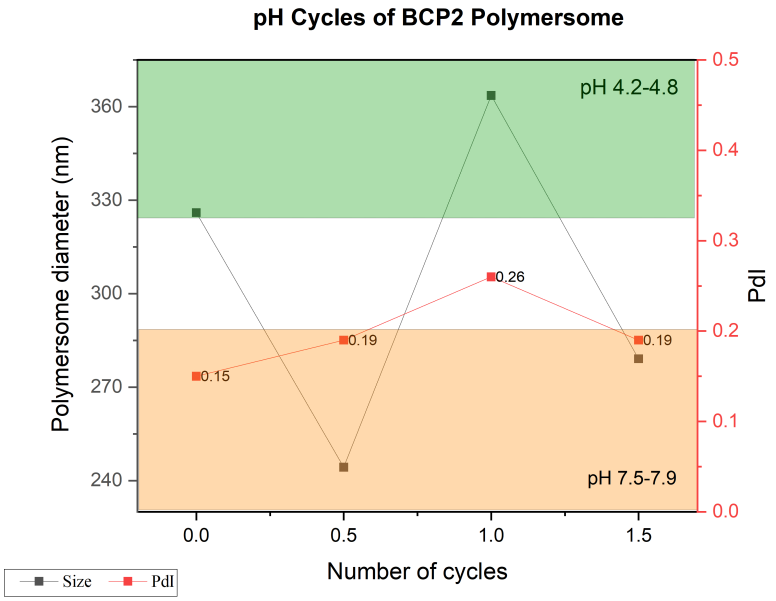

Figure 4.11. pH Cycle Study of Ferrocene Containing Polymersomes Produced from BCP2.

4.2.2 Morphological Characterization

In this part, STEM images of Empty Ferrocene-free Polymersomes (FFP) and Empty Ferrocene-containing Polymersomes (FCP) that were obtained for morphological evaluation are presented, as seen Figure 4.12.

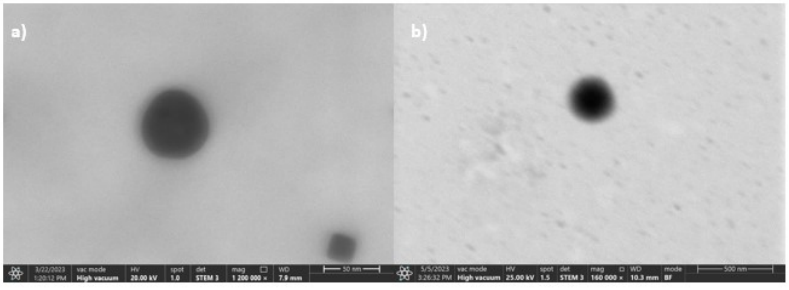

Figure 4.12. a) STEM image of Empty Ferrocene-Free Polymersome at a 50 nm scale. b) STEM image of Empty Ferrocene-Containing Polymersome at a 500 nm scale.

The morphological characteristics, which are widely visible in these photos, contribute to a detailed understanding of the inherent properties of such polymersomes. In addition, a STEM image has been obtained of the interactions between FCP and SPIONs which will be presented for further section.

4.3 Characterization Results of SPION-Polymersome Interactions

Both Ferrocene-containing and Ferrocene-free polymersomes were subjected to interaction with β-CD coated SPIONs to evaluate the dynamics of their association and responsiveness. The detailed characterisation results of such interactions shall be discussed in this section,with a view to providing insight into their particular properties and possible applications for complex nanosystems.

4.3.1 Size and Polydispersity Index Measurement

As outlined in Section 3.2.5, an experiment was conducted to test the interaction between β-CD coated SPIONs and polymersomes.The Ferrocene-Free Polymersome were the primary focus of the first analysis. It was assumed that the β-CD coated SPIONs would not interact in any significant capacity to Ferrocene-Free Polymersome. During this experiment, DLS measurements were performed to determine the size of polymersomes that had been interacting with a β-CD coated SPIONs. Furthermore, the resulting sample followed by centrifugation at 4000 rpm for 15 minutes and re-measured using DLS. After centrifugation, the resulting sample did not exhibit the anticipated phase separation into distinct pellet and supernatant fractions. Surprisingly, an orange precipitate formed, adhering to the inner wall of the Eppendorf tube and remaining insoluble in water. This peculiar observation led us to infer that the precipitate was likely composed of unbound SPIONs that had not undergone interactions with the polymersomes. Subsequently, the upper portion of the Eppendorf tube, which can be referred to as the supernatant, was subjected to analysis using DLS. In order to ensure the accuracy of subsequent measurements and analysis, this process has been used to remove any unbound or agglomerated SPIONs. The results of this study are summarized in Table 4.4.

Table 4.4. Hydrodynamic Size and PdI of the Ferrocene-Free Polymersome (FFP) interacting with the β-CD coated SPIONs

Sample	Size (nm)	PDI
β-CD coated SPIONs + FFP	66.16±1.03	0.19±0.013
β-CD coated SPIONs + FFP (Supernatant)	68.88±0.40	0.21±0.008

Following the interaction between FFP and SPIONs, no significant change was observed when compared to the Empty FFP. The result confirms the initial assumption that there would be no significant interaction between β-CD coated SPIONs and FFPs.

It is also noteworthy that following the interaction and centrifugation processes, unbound β-CD coated SPIONs were visually detected as a yellowish residue adhering to the inner surfaces of both the glass flask and the eppendorf tube used. These residues were unable to be analyzed due to their adhesion to the container walls.

Subsequently the aforementioned procedure conducted with FFP, a similar analysis was carried out with FCP. The same steps have also been repeated, including interaction with β-CD coated SPIONs, measurement of DLS, centrifugation and subsequent DLSC re-measurement. In this process, however, a major distinction has emerged; the FCP sample was divided into separate supernatant and pellet phases after centrifugation. The characterisation of the FCP and its interaction with SPIONs was further supported by this separtation. Table 4.5 summarises the results of that analysis.

Table 4.5. Hydrodynamic Size and PDI of the Ferrocene-Containing Polymersome (FCP) interacting with the β-CD coated SPIONs

Sample	Size (nm)	PDI
β-CD coated SPIONs + FCP	990±141.7	0.25±0.018
β-CD coated SPIONs + FCP (Re-dispersed pellet)	1260±292.8	0.51± 0.184
β-CD coated SPIONs + FCP (Supernatant)	849±102.3	0.55 ± 0.01

Compared to the FFP, the FCP showed a marked increase in size following its interaction with the SPIONs. The size that was significantly increased after the inter-

action with SPIONs implies that there was a strong interaction between the Ferrocene units in FCP and the β-CD coating on SPIONs. It seems that this interaction is facilitating the aggregation of SPIONs, resulting in an increase in aggregate formation.

4.3.2 Morphological Characterization

Further morphological examination was deemed important in light of the significant size increase for the FCP that was measured by DLS. This analysis was based on STEM, a method providing higher resolution and facilitating more detailed investigations into the structure of polymersomes after interaction. Figure 4.13 shows the visual representation of this interaction. These figures highlight the significant interaction between FCP and SPIONs, which further enhances our understanding of these complex systems.

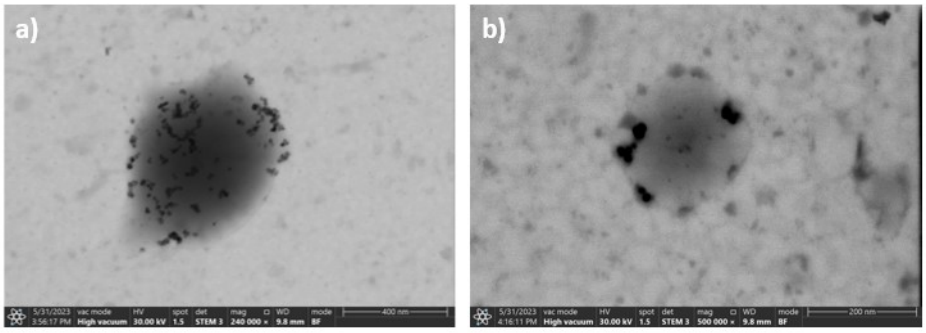

Figure 4.13. STEM analysis of SPION-Interacted Ferrocene-Containing Polymersome.

In addition, a re-dispersed pellet sample which had been centrifuged at 4000 rpm for 15 minutes was analysed with STEM, as seen Figure 4.14. The results of this analysis demonstrated that the polymersomes continued to interact with β-CD coated SPIONs on their surface post-centrifugation. This persistent interaction indicates that β-CD coated SPIONs are rigidly attached to the polymer surface in spite of physical and technical hinders such as centrifugation. These phenomena highlight the substantial role that these particles play in changing polymersomes properties, which can have a potential impact on their function in subsequent applications.

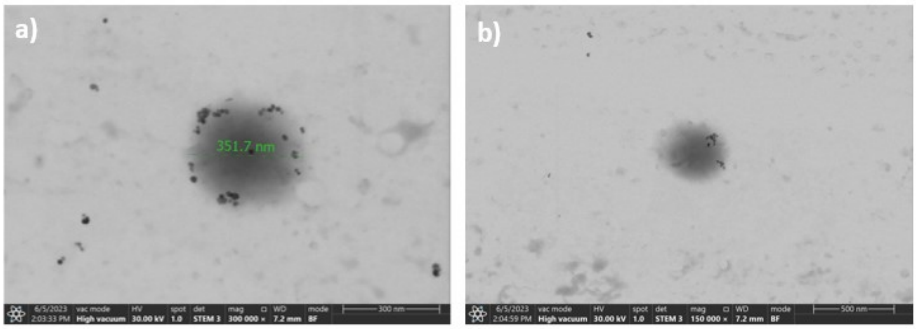

Figure 4.14. STEM Analysis of Re-dispersed Ferrocene-Containing Polymersome' Pellet After Centrifugation.

In conclusion, it was demonstrated that their interactions with the FCP and β-CD coated SPIONs have been observed to be active on the polymersome surface following centrifugation as well as influencing the morphology of the whole polymersome. Opportunities for further research exist in the robustness of these interactions, as well as their possible implications for other applications of such polymersome systems.

5. CONCLUSIONS AND OUTLOOK

5.1 Conclusions

In this thesis, β-Cyclodextrin coated Superparamagnetic Iron Oxide Nanoparticles were synthesized by co-precipitation technique. Subsequently, Ferrocene-Containing Polymersomes were produced and interacted with these β-Cyclodextrin coated Superparamagnetic Iron Oxide Nanoparticles.

The Leibniz Institute of Polymer Research Dresden generously provided the block copolymers used in these studies. Experiments and analyses were carefully performed across two distinguished institutions: At Leibniz Institute of Polymer Research Dresden, part of this work has been carried out and the subsequent studies have taken place at BINDLAB in the Department of Biomedical Engineering Boğaziçi University. This comprehensive study has brought to light the following important findings and conclusions: :

1. β-Cyclodextrin coated Superparamagnetic Iron Oxide Nanoparticles were synthesized by co-precipitation technique. The nanoparticles were characterized by DLS, TEM, TGA, FTIR and VSM techniques and showed good magnetic properties and stability.

2. TEM analyzes of the β-CD coated SPIONs has been carried out in order to verify their size and morphology. A clear overview of the SPIONs was easy to achieve as a result of its high contrast.

3. The PBS buffer has been used for the purpose of ensuring that β-CD coated SPIONs are stable at pH 7.4. The DLS measurements confirmed the stability and dispersibility of the nanoparticles in the buffer solution.

4. The distribution of polymersome size by DLS measurements has been quantified, with a narrow distribution and consistent repeatability demonstrating the

robustness of the synthesis method used.

5. The pH-responsive nature of the polymersomes was investigated using pH titration. In particular, an increase in size was observed under acid conditions, whereas there was a decrease in the alkaline environment. The potential of these polymersomes for targeted drug release in pH dependent cellular compartments is highlighted by this behaviour.

6. DLS analysis showed that the interactions between the Ferrocene-Free Polymersome and the β-CD coated SPIONs did not provide a result that could be distinguished from the empty Ferrocene-Free Polymersome . This suggests that the ferrocene is essential for the binding of the β-CD coated SPIONs.

7. STEM images of Ferrocene-Containing Polymersomes that interacted with β-CD coated SPIONs clearly demonstrate the persistent association between them even after centrifugation. Adjacent to the polymersome structures, black spheroidal formations with diameters in the range of 10-12 nm were evident. It was clear from these formations that they were β-CD coated SPIONs, both in their characteristic size as well as the increased contrast.

5.2 Future Directions in Research

This study has laid a foundational groundwork for the design of innovative multi-responsive drug delivery systems, which are able to use both pH-responsive behavior and magnetic properties. There are several possibilities for further research and optimization with the unique system described here. Encapsulating hydrophilic anti-cancer drugs into the polymersome's core is one possible promising approach. In contrast, hydrophobic drugs might be kept within the hydrophobic cavities of β-Cyclodextrin. This strategy could potentially enable the simultaneous administration of many drugs with various solubility profiles, resolving a long-standing problem in the field of drug delivery.

Additionally, a polymersome system with magnetic characteristics developed from this study could improve targeted drug delivery. In this way, the challenges frequently associated with conventional chemotherapy, such as broad toxicity and unfavorable side effects as a result of non-targeted delivery, can be significantly minimized.

In conclusion, the current study opens the way for the development of a cutting-edge drug delivery system that is not only responsive to multiple stimuli but also flexible enough to preserve a variety of therapeutic agents. The applicability of these systems to personalised health care is vast and the development of such research suggests that groundbreaking solutions can be achieved for a large number of clinical problems.

REFERENCES

1. Sung, H., J. Ferlay, R. L. Siegel, M. Laversanne, I. Soerjomataram, A. Jemal and F. Bray, "Global cancer statistics 2020: GLOBOCAN estimates of incidence and mortality worldwide for 36 cancers in 185 countries", *CA: A Cancer Journal for Clinicians*, Vol. 71, No. 3, pp. 209–249, 2021.

2. Mokhtari, R. B., T. S. Homayouni, N. Baluch, E. Morgatskaya, S. Kumar, B. Das and H. Yeger, "Combination therapy in combating cancer", *Oncotarget*, Vol. 8, No. 23, p. 38022, 2017.

3. Hassan, M., H. Watari, A. AbuAlmaaty, Y. Ohba, N. Sakuragi *et al.*, "Apoptosis and molecular targeting therapy in cancer", *BioMed Research International*, Vol. 2014, 2014.

4. Jain, V., S. Jain and S. Mahajan, "Nanomedicines based drug delivery systems for anticancer targeting and treatment", *Current Drug Delivery*, Vol. 12, No. 2, pp. 177–191, 2015.

5. Silva, A. K., N. Luciani, F. Gazeau, K. Aubertin, S. Bonneau, C. Chauvierre, D. Letourneur and C. Wilhelm, "Combining magnetic nanoparticles with cell derived microvesicles for drug loading and targeting", *Nanomedicine: Nanotechnology, Biology and Medicine*, Vol. 11, No. 3, pp. 645–655, 2015.

6. Purushotham, S., P. Chang, H. Rumpel, I. Kee, R. Ng, P. Chow, C. Tan and R. Ramanujan, "Thermoresponsive core–shell magnetic nanoparticles for combined modalities of cancer therapy", *Nanotechnology*, Vol. 20, No. 30, p. 305101, 2009.

7. Senyei, A., K. Widder and G. Czerlinski, "Magnetic guidance of drug-carrying microspheres", *Journal of Applied Physics*, Vol. 49, No. 6, pp. 3578–3583, 1978.

8. Weinberg, R. A., "How cancer arises", *Scientific American*, Vol. 275, No. 3, pp. 62–70, 1996.

9. Crosby, D., S. Bhatia, K. M. Brindle, L. M. Coussens, C. Dive, M. Emberton, S. Esener, R. C. Fitzgerald, S. S. Gambhir, P. Kuhn *et al.*, "Early detection of cancer", *Science*, Vol. 375, No. 6586, p. eaay9040, 2022.

10. Kubota, K., "Recent advances and limitations of surgical treatment for pancreatic cancer", *World Journal of Clinical Oncology*, Vol. 2, No. 5, p. 225, 2011.

11. König, J., R. van Ewijk, K. Kuhr, H. Schmidberger, A. Wöckel, R. Kreienberg and M. Blettner, "Radiotherapy effects on early breast cancer survival in observational and randomized studies: a systematic analysis of advantages, disadvantages and differences between the two study types", *Breast Cancer*, Vol. 23, pp. 415–424, 2016.

12. Pearce, A., M. Haas, R. Viney, S.-A. Pearson, P. Haywood, C. Brown and R. Ward, "Incidence and severity of self-reported chemotherapy side effects in routine care: A prospective cohort study", *Plos One*, Vol. 12, No. 10, p. e0184360, 2017.

13. Toumey, C., "Plenty of room, plenty of history", *Nature Nanotechnology*, Vol. 4, No. 12, pp. 783–784, 2009.

14. Taniguchi, N., "On the basic concept of nano-technology proceedings of the international conference on production engineering tokyo part ii japan society of precision engineering", *Japan Society of Precision Engineering*, 1974.

15. Brambilla, D., P. Luciani and J.-C. Leroux, "Breakthrough discoveries in drug delivery technologies: the next 30 years", *Journal of Controlled Release*, Vol. 190, pp. 9–14, 2014.

16. Oylar, Ö. and İ. Tekin, "Kanserin teşhis ve tedavisinde nanoteknolojinin önemi", *Uludağ Üniversitesi Mühendislik Fakültesi Dergisi*, Vol. 16, No. 1, 2011.

17. Peppas, N. A., "Historical perspective on advanced drug delivery: How engineering design and mathematical modeling helped the field mature", *Advanced Drug Delivery Reviews*, Vol. 65, No. 1, pp. 5–9, 2013.

18. Polo, E., M. Collado, B. Pelaz and P. Del Pino, "Advances toward more efficient targeted delivery of nanoparticles in vivo: understanding interactions between nanoparticles and cells", *ACS Nano*, Vol. 11, No. 3, pp. 2397–2402, 2017.

19. Giamberti, A., F. Caldaroni, A. Varrica, C. Pace Napoleone, S. M. Marianeschi, N. Uricchio, V. Vanini, F. Santoro, G. B. Luciani, G. Stellin *et al.*, "Impact of COVID-19 pandemic on the Italian humanitarian congenital cardiac surgery activity: What no one tells you", *Frontiers in Cardiovascular Medicine*, Vol. 8, p. 705029, 2021.

20. Karabasz, A., M. Bzowska and K. Szczepanowicz, "Biomedical applications of multifunctional polymeric nanocarriers: A review of current literature", *International Journal of Nanomedicine*, pp. 8673–8696, 2020.

21. Plapied, L., N. Duhem, A. des Rieux and V. Préat, "Fate of polymeric nanocarriers for oral drug delivery", *Current Opinion in Colloid & Interface Science*, Vol. 16, No. 3, pp. 228–237, 2011.

22. Bawarski, W. E., E. Chidlowsky, D. J. Bharali and S. A. Mousa, "Emerging nanopharmaceuticals", *Nanomedicine: Nanotechnology, Biology and Medicine*, Vol. 4, No. 4, pp. 273–282, 2008.

23. Kothamasu, P., H. Kanumur, N. Ravur, C. Maddu, R. Parasuramrajam and S. Thangavel, "Nanocapsules: the weapons for novel drug delivery systems", *BioImpacts: BI*, Vol. 2, No. 2, p. 71, 2012.

24. Iyisan, B. and K. Landfester, "Polymeric nanocarriers", *Biological Responses to Nanoscale Particles: Molecular and Cellular Aspects and Methodological Approaches*, pp. 53–84, 2019.

25. Kowalczuk, A., R. Trzcinska, B. Trzebicka, A. H. Müller, A. Dworak and C. B. Tsvetanov, "Loading of polymer nanocarriers: Factors, mechanisms and applications", *Progress in Polymer Science*, Vol. 39, No. 1, pp. 43–86, 2014.

26. Rytting, E., J. Nguyen, X. Wang and T. Kissel, "Biodegradable polymeric nanocarriers for pulmonary drug delivery", *Expert opinion on Drug Delivery*, Vol. 5, No. 6, pp. 629–639, 2008.

27. So, S. and T. P. Lodge, "Size control and fractionation of ionic liquid filled polymersomes with glassy and rubbery bilayer membranes", *Langmuir*, Vol. 32, No. 19, pp. 4959–4968, 2016.

28. Levine, D. H., P. P. Ghoroghchian, J. Freudenberg, G. Zhang, M. J. Therien, M. I. Greene, D. A. Hammer and R. Murali, "Polymersomes: a new multi-functional tool for cancer diagnosis and therapy", *Methods*, Vol. 46, No. 1, pp. 25–32, 2008.

29. Discher, B. M., Y.-Y. Won, D. S. Ege, J. C. Lee, F. S. Bates, D. E. Discher and D. A. Hammer, "Polymersomes: tough vesicles made from diblock copolymers", *Science*, Vol. 284, No. 5417, pp. 1143–1146, 1999.

30. LoPresti, C., H. Lomas, M. Massignani, T. Smart and G. Battaglia, "Polymersomes: nature inspired nanometer sized compartments", *Journal of Materials Chemistry*, Vol. 19, No. 22, pp. 3576–3590, 2009.

31. Anajafi, T., M. D. Scott, S. You, X. Yang, Y. Choi, S. Y. Qian and S. Mallik, "Acridine orange conjugated polymersomes for simultaneous nuclear delivery of gemcitabine and doxorubicin to pancreatic cancer cells", *Bioconjugate Chemistry*, Vol. 27, No. 3, pp. 762–771, 2016.

32. Hu, M., Y. Shen, L. Zhang and L. Qiu, "Polymersomes via self-assembly of amphiphilic β-cyclodextrin-centered triarm star polymers for enhanced oral bioavailability of water-soluble chemotherapeutics", *Biomacromolecules*, Vol. 17, No. 3, pp. 1026–1039, 2016.

33. Zhang, X.-y. and P.-y. Zhang, "Polymersomes in nanomedicine-A review", *Current Nanoscience*, Vol. 13, No. 2, pp. 124–129, 2017.

34. Poma, A., Y. Pei, L. Ruiz-Perez, L. Rizzello and G. Battaglia, "Polymersomes: Synthesis and applications", *Encyclopedia of Polymer Science and Technology*, pp. 1–43, 2002.

35. Lefley, J., C. Waldron and C. R. Becer, "Macromolecular design and preparation of polymersomes", *Polymer Chemistry*, Vol. 11, No. 45, pp. 7124–7136, 2020.

36. Carlsen, A., N. Glaser, J.-F. Le Meins and S. Lecommandoux, "Block copolymer vesicle permeability measured by osmotic swelling and shrinking", *Langmuir*, Vol. 27, No. 8, pp. 4884–4890, 2011.

37. Kumar, M., M. Grzelakowski, J. Zilles, M. Clark and W. Meier, "Highly permeable polymeric membranes based on the incorporation of the functional water channel protein Aquaporin Z", *Proceedings of the National Academy of Sciences*, Vol. 104, No. 52, pp. 20719–20724, 2007.

38. Utada, A. S., E. Lorenceau, D. R. Link, P. D. Kaplan, H. A. Stone and D. Weitz, "Monodisperse double emulsions generated from a microcapillary device", *Science*, Vol. 308, No. 5721, pp. 537–541, 2005.

39. Danafar, H., K. Rostamizadeh, S. Davaran and M. Hamidi, "PLA-PEG-PLA copolymer-based polymersomes as nanocarriers for delivery of hydrophilic and hydrophobic drugs: preparation and evaluation with atorvastatin and lisinopril", *Drug Development and Industrial Pharmacy*, Vol. 40, No. 10, pp. 1411–1420, 2014.

40. Kim, M. R. and I. W. Cheong, "Stimuli-triggered Formation of Polymersomes from W/O/W Multiple Double Emulsion Droplets Containing Poly (styrene)-block-poly (N-isopropylacrylamide-co-spironaphthoxazine methacryloyl)", *Langmuir*, Vol. 32, No. 36, pp. 9223–9228, 2016.

41. Meeuwissen, S. A., K. T. Kim, Y. Chen, D. J. Pochan and J. C. van Hest, "Controlled shape transformation of polymersome stomatocytes", *Angewandte Chemie*, Vol. 123, No. 31, pp. 7208–7211, 2011.

42. Charleux, B., G. Delaittre, J. Rieger and F. D'Agosto, "Polymerization-induced self-assembly: from soluble macromolecules to block copolymer nano-objects in one step", *Macromolecules*, Vol. 45, No. 17, pp. 6753–6765, 2012.

43. Iyisan, B., J. Kluge, P. Formanek, B. Voit and D. Appelhans, "Multifunctional and dual-responsive polymersomes as robust nanocontainers: design, formation by sequential post-conjugations, and pH-controlled drug release", *Chemistry of Materials*, Vol. 28, No. 5, pp. 1513–1525, 2016.

44. De Oliveira, H., J. Thevenot and S. Lecommandoux, "Smart polymersomes for therapy and diagnosis: fast progress toward multifunctional biomimetic nanomedicines", *Wiley Interdisciplinary Reviews: Nanomedicine and Nanobiotechnology*, Vol. 4, No. 5, pp. 525–546, 2012.

45. Bulte, J. W. and D. L. Kraitchman, "Iron oxide MR contrast agents for molecular and cellular imaging", *NMR in Biomedicine: An International Journal Devoted to the Development and Application of Magnetic Resonance In Vivo*, Vol. 17, No. 7, pp. 484–499, 2004.

46. Wu, K., D. Su, J. Liu, R. Saha and J.-P. Wang, "Magnetic nanoparticles in nanomedicine: a review of recent advances", *Nanotechnology*, Vol. 30, No. 50, p. 502003, 2019.

47. Martins, P. M., A. C. Lima, S. Ribeiro, S. Lanceros-Mendez and P. Martins, "Magnetic nanoparticles for biomedical applications: from the soul of the earth to the deep history of ourselves", *ACS Applied Bio Materials*, Vol. 4, No. 8, pp. 5839–5870, 2021.

48. Kaufman, A. A., R. O. Hansen and R. L. Kleinberg, "Paramagnetism, Diamagnetism, and Ferromagnetism", *Methods in Geochemistry and Geophysics*, Vol. 42, pp. 207–254, 2008.

49. Jian, X., J. Qin and Q. Gu, "Diamagnetism versus paramagnetism in charged spin-1 Bose gases", *Journal of Physics: Condensed Matter*, Vol. 23, No. 2, p. 026003, 2010.

50. Nalwa, H. S., *Encyclopedia of nanoscience and nanotechnology*, American Scientific Publishers, 2004.

51. Leslie-Pelecky, D. L. and R. D. Rieke, "Magnetic properties of nanostructured materials", *Chemistry of Materials*, Vol. 8, No. 8, pp. 1770–1783, 1996.

52. Xu, C. and S. Sun, "New forms of superparamagnetic nanoparticles for biomedical applications", *Advanced Drug Delivery Reviews*, Vol. 65, No. 5, pp. 732–743, 2013.

53. Cardoso, V. F., A. Francesko, C. Ribeiro, M. Bañobre-López, P. Martins and S. Lanceros-Mendez, "Advances in magnetic nanoparticles for biomedical applications", *Advanced Healthcare Materials*, Vol. 7, No. 5, p. 1700845, 2018.

54. Liu, S., B. Yu, S. Wang, Y. Shen and H. Cong, "Preparation, surface functionalization and application of Fe3O4 magnetic nanoparticles", *Advances in Colloid and Interface Science*, Vol. 281, p. 102165, 2020.

55. Roy, I. and K. Kritika, "Therapeutic applications of magnetic nanoparticles: recent advances", *Materials Advances*, 2022.

56. Hedayatnasab, Z., F. Abnisa and W. M. A. W. Daud, "Review on magnetic nanoparticles for magnetic nanofluid hyperthermia application", *Materials & Design*, Vol. 123, pp. 174–196, 2017.

57. Anik, M. I., M. K. Hossain, I. Hossain, A. Mahfuz, M. T. Rahman and I. Ahmed, "Recent progress of magnetic nanoparticles in biomedical applications: A review", *Nano Select*, Vol. 2, No. 6, pp. 1146–1186, 2021.

58. Mosayebi, J., M. Kiyasatfar and S. Laurent, "Synthesis, functionalization, and design of magnetic nanoparticles for theranostic applications", *Advanced Healthcare Materials*, Vol. 6, No. 23, p. 1700306, 2017.

59. Gan, Y. X., A. H. Jayatissa, Z. Yu, X. Chen and M. Li, "Hydrothermal synthesis of nanomaterials", *Journal of Nanomaterials*, Vol. 2020, pp. 1–3, 2020.

60. Niculescu, A.-G., C. Chircov and A. M. Grumezescu, "Magnetite nanoparticles: Synthesis methods–A comparative review", *Methods*, Vol. 199, pp. 16–27, 2022.

61. Majidi, S., F. Zeinali Sehrig, S. M. Farkhani, M. Soleymani Goloujeh and A. Akbarzadeh, "Current methods for synthesis of magnetic nanoparticles", *Artificial Cells, Nanomedicine, and Biotechnology*, Vol. 44, No. 2, pp. 722–734, 2016.

62. Singh, N., G. J. Jenkins, R. Asadi and S. H. Doak, "Potential toxicity of superparamagnetic iron oxide nanoparticles (SPION)", *Nano Reviews*, Vol. 1, No. 1, p. 5358, 2010.

63. Ali, A., H. Zafar, M. Zia, I. ul Haq, A. R. Phull, J. S. Ali and A. Hussain, "Synthesis, characterization, applications, and challenges of iron oxide nanoparticles", *Nanotechnology, Science and Applications*, pp. 49–67, 2016.

64. Petri-Fink, A., M. Chastellain, L. Juillerat-Jeanneret, A. Ferrari and H. Hofmann, "Development of functionalized superparamagnetic iron oxide nanoparticles for interaction with human cancer cells", *Biomaterials*, Vol. 26, No. 15, pp. 2685–2694, 2005.

65. Wahajuddin, n. and S. Arora, "Superparamagnetic iron oxide nanoparticles: magnetic nanoplatforms as drug carriers", *International Journal of Nanomedicine*, pp. 3445–3471, 2012.

66. Wu, W., Z. Wu, T. Yu, C. Jiang and W.-S. Kim, "Recent progress on magnetic iron oxide nanoparticles: synthesis, surface functional strategies and biomedical applications", *Science and Technology of Advanced Materials*, Vol. 16, No. 2, p. 023501, 2015.

67. Dave, S. R. and X. Gao, "Monodisperse magnetic nanoparticles for biodetection, imaging, and drug delivery: a versatile and evolving technology", *Wiley Interdisciplinary Reviews: Nanomedicine and Nanobiotechnology*, Vol. 1, No. 6, pp. 583–609, 2009.

68. Massart, R., "Preparation of aqueous magnetic liquids in alkaline and acidic media", *IEEE Transactions on Magnetics*, Vol. 17, No. 2, pp. 1247–1248, 1981.

69. Wulandari, I., D. Santjojo, R. Shobirin and A. Sabarudin, "Characteristics and magnetic properties of chitosan-coated Fe3O4 nanoparticles prepared by ex-situ co-precipitation method", *Rasayan J. Chem*, Vol. 10, pp. 1348–1358, 2017.

70. Tartaj, P., M. del Puerto Morales, S. Veintemillas-Verdaguer, T. González-Carreño and C. J. Serna, "The preparation of magnetic nanoparticles for applications in biomedicine", *Journal of Physics D: Applied Physics*, Vol. 36, No. 13, p. R182, 2003.

71. Stanicki, D., L. Vander Elst, R. N. Muller and S. Laurent, "Synthesis and processing of magnetic nanoparticles", *Current Opinion in Chemical Engineering*, Vol. 8, pp. 7–14, 2015.

72. Sodipo, B. K. and A. A. Aziz, "Recent advances in synthesis and surface modification of superparamagnetic iron oxide nanoparticles with silica", *Journal of Magnetism and Magnetic Materials*, Vol. 416, pp. 275–291, 2016.

73. Jin, R., B. Lin, D. Li and H. Ai, "Superparamagnetic iron oxide nanoparticles for MR imaging and therapy: design considerations and clinical applications", *Current Opinion in Pharmacology*, Vol. 18, pp. 18–27, 2014.

74. Li, H., M. H. El-Dakdouki, D. C. Zhu, G. S. Abela and X. Huang, "Synthesis of β-cyclodextrin conjugated superparamagnetic iron oxide nanoparticles for selective binding and detection of cholesterol crystals", *Chemical Communications*, Vol. 48, No. 28, pp. 3385–3387, 2012.

75. Racuciu, M., D. Creanga, V. Badescu and A. Airinei, "Synthesis and physical characterization of magnetic nano-particles functionalized with beta-cyclodextrin", *Journal of Optoelectronics and Advanced Materials*, Vol. 9, No. 5, p. 1530, 2007.

76. Szejtli, J., "Introduction and general overview of cyclodextrin chemistry", *Chemical Reviews*, Vol. 98, No. 5, pp. 1743–1754, 1998.

77. Crini, G., "A history of cyclodextrins", *Chemical Reviews*, Vol. 114, No. 21, pp. 10940–10975, 2014.

78. Morin-Crini, N., S. Fourmentin, É. Fenyvesi, E. Lichtfouse, G. Torri, M. Fourmentin and G. Crini, "130 years of cyclodextrin discovery for health, food, agriculture, and the industry: A review", *Environmental Chemistry Letters*, Vol. 19, pp. 2581–2617, 2021.

79. Davis, M. E. and M. E. Brewster, "Cyclodextrin-based pharmaceutics: past, present and future", *Nature Reviews Drug Discovery*, Vol. 3, No. 12, pp. 1023–1035, 2004.

80. Voncina, B. and V. Vivod, "Cyclodextrins in textile finishing", *Eco-friendly Textile Dyeing and Finishing*, pp. 53–75, 2013.

81. Bezerra, F. M., M. J. Lis, H. B. Firmino, J. G. Dias da Silva, R. d. C. S. Curto Valle, J. A. Borges Valle, F. A. P. Scacchetti and A. L. Tessaro, "The role of β-cyclodextrin in the textile industry", *Molecules*, Vol. 25, No. 16, p. 3624, 2020.

82. Jambhekar, S. S. and P. Breen, "Cyclodextrins in pharmaceutical formulations I: Structure and physicochemical properties, formation of complexes, and types of complex", *Drug Discovery Today*, Vol. 21, No. 2, pp. 356–362, 2016.

83. Poulson, B. G., Q. A. Alsulami, A. Sharfalddin, E. F. El Agammy, F. Mouffouk, A.-H. Emwas, L. Jaremko and M. Jaremko, "Cyclodextrins: Structural, chemical, and physical properties, and applications", *Polysaccharides*, Vol. 3, No. 1, pp. 1–31, 2021.

84. Connors, K. A., "The stability of cyclodextrin complexes in solution", *Chemical Reviews*, Vol. 97, No. 5, pp. 1325–1358, 1997.

85. on Food Additives, E. P., N. S. added to Food (ANS), A. Mortensen, F. Aguilar, R. Crebelli, A. Di Domenico, B. Dusemund, M. J. Frutos, P. Galtier, D. Gott, U. Gundert-Remy *et al.*, "Re-evaluation of β-cyclodextrin (E 459) as a food additive", *EFSA Journal*, Vol. 14, No. 12, p. e04628, 2016.

86. Bhaskara-Amrit, U. R., P. B. Agrawal and M. Warmoeskerken, "Applications of β-cyclodextrins in textiles", *Autex Res. J*, Vol. 11, No. 4, pp. 94–101, 2011.

87. Ayşe, A. and S. Dönmez, "Siklodekstrinler ve gıda endüstrisinde kullanımları", *Gıda*, Vol. 35, No. 4, pp. 305–316, 2010.

88. Szejtli, J., "Utilization of cyclodextrins in industrial products and processes", *Journal of Materials Chemistry*, Vol. 7, No. 4, pp. 575–587, 1997.

89. Paudel, A., Z. A. Worku, J. Meeus, S. Guns and G. Van den Mooter, "Manufacturing of solid dispersions of poorly water soluble drugs by spray drying: formulation and process considerations", *International Journal of Pharmaceutics*, Vol. 453, No. 1, pp. 253–284, 2013.

90. D'souza, A. A. and R. Shegokar, "Polyethylene glycol (PEG): a versatile polymer for pharmaceutical applications", *Expert Opinion on Drug Delivery*, Vol. 13, No. 9, pp. 1257–1275, 2016.

91. Knop, K., R. Hoogenboom, D. Fischer and U. S. Schubert, "Poly (ethylene glycol) in drug delivery: pros and cons as well as potential alternatives", *Angewandte Chemie International Edition*, Vol. 49, No. 36, pp. 6288–6308, 2010.

92. Anajafi, T. and S. Mallik, "Polymersome-based drug-delivery strategies for cancer therapeutics", *Therapeutic Delivery*, Vol. 6, No. 4, pp. 521–534, 2015.

93. Zhou, D., Z. Fei, L. Jin, P. Zhou, C. Li, X. Liu and C. Zhao, "Dual-responsive polymersomes as anticancer drug carriers for the co-delivery of doxorubicin and paclitaxel", *Journal of Materials Chemistry B*, Vol. 9, No. 3, pp. 801–808, 2021.

94. Van Staveren, D. R. and N. Metzler-Nolte, "Bioorganometallic chemistry of ferrocene", *Chemical Reviews*, Vol. 104, No. 12, pp. 5931–5986, 2004.

95. Patra, M. and G. Gasser, "The medicinal chemistry of ferrocene and its derivatives", *Nature Reviews Chemistry*, Vol. 1, No. 9, p. 0066, 2017.

96. Wang, D., S. Moreno, S. Boye, B. Voit and D. Appelhans, "Crosslinked and Multi-Responsive Polymeric Vesicles as a Platform to Study Enzyme-Mediated Undocking Behavior: Toward Future Artificial Organelle Communication", *Macromolecular Rapid Communications*, p. 2200885, 2023.

97. Moreno, S., H. Hu¨bner, C. Effenberg, S. Boye, A. Ramuglia, D. Schmitt, B. Voit, I. M. Weidinger, M. Gallei and D. Appelhans, "Redox-and pH-Responsive Polymersomes with Ferrocene Moieties Exhibiting Peroxidase-like, Chemoenzymatic Activity and H2O2-Responsive Release Behavior", *Biomacromolecules*, Vol. 23, No. 11, pp. 4655–4667, 2022.

98. Krishnakumar, G. S., S. Sampath, S. Muthusamy and M. A. John, "Importance of crosslinking strategies in designing smart biomaterials for bone tissue engineering: A systematic review", *Materials Science and Engineering: C*, Vol. 96.

99. Gaitzsch, J., I. Canton, D. Appelhans, G. Battaglia and B. Voit, "Cellular interactions with photo-cross-linked and pH-sensitive polymersomes: biocompatibility and uptake studies", *Biomacromolecules*, Vol. 13, No. 12, pp. 4188–4195, 2012.

100. Hamza, H., A. M. Ferretti, C. Innocenti, K. Fidecka, E. Licandro, C. Sangregorio and D. Maggioni, "An approach for magnetic halloysite nanocomposite with selective loading of superparamagnetic magnetite nanoparticles in the lumen", *Inorganic Chemistry*, Vol. 59, No. 17, pp. 12086–12096, 2020.